3-29-2022

Development of the UHPC Mix for 3D Printing

Buse Ilayda Oz
Florida International University, boz001@fiu.edu

FLORIDA INTERNATIONAL UNIVERSITY

Miami, Florida

DEVELOPMENT OF THE UHPC MIX FOR 3D PRINTING

A thesis submitted in partial fulfillment of

the requirements for the degree of

MASTER OF SCIENCE

in

CIVIL ENGINEERING

by

Buse Ilayda Oz

2022

To: Dean John L. Volakis
College of Engineering and Computing

This thesis, written by Buse Ilayda Oz, and entitled Development of the UHPC Mix for 3D Printing, having been approved in respect to style and intellectual content, is referred to you for judgment.

We have read this thesis and recommend that it be approved.

_____
Kingsley Lau

_____
Amal Elawady

_____
Wallied Orabi

_____
Atorod Azizinamini, Major Professor

Date of Defense: March 29, 2022

The thesis of Buse Ilayda Oz is approved.

_____
Dean John L. Volakis
College of Engineering and Computing

_____
Andrés G. Gil
Vice President for Research and Economic Development
and Dean of the University Graduate School

Florida International University, 2022

ACKNOWLEDGMENTS

I would like to thank my supervisor Dr. Atorod Azizinamini, as well as Dr. Islam Mantawy for their assistance and advice throughout this thesis research. Without their assistance and dedicated involvement in every step throughout the process, this paper would have never been accomplished. I also would like to convey my heartfelt gratitude to my family and partner for their unwavering support and encouragement throughout my years of education, as well as during the research and writing of this thesis. Without them, this accomplishment would not have been possible.

.

ABSTRACT OF THE THESIS

DEVELOPMENT OF THE UHPC MIX FOR 3D PRINTING

by

Buse Ilayda Oz

Florida International University, 2022

Miami, Florida

Professor Atorod Azizinamini, Major Professor

This thesis utilizes the development of Ultra-High-Performance Concrete mix design for 3 Dimensional (3D) Printing purposes. 3D concrete printing offers many advantages such as improvements in safety, quality, and productivity. Moreover, it holds a great advantage for the construction of structural elements that are difficult to construct by conventional methods. These advantages carry a huge potential for solving the aforementioned challenges. Seven UHPC mixes have been designed and analyzed using various test setups for comparison purposes. Extrudability, flowability, buildability, and open time were measured using the fresh properties of the UHPC mixes. Mechanical properties were measured using compression test setups. The optimum mix design has reached up to 18 inches before the collapse. This mix has achieved an average 28 days strength of 17.25 ksi with a flowability value of 4.5 inches.

TABLE OF CONTENTS

CHAPTER PAGE

LIST OF TABLES

TABLE PAGE

LIST OF FIGURES

FIGURE PAGE

1 INTRODUCTION

1.1. Problem Statement

Over the past decade, robotics and automation techniques have been commonly employed in numerous fields such as automotive, aerospace, and electronics due to their enormous production and design standardization capabilities. This accelerating interest in robotic technology as well as the increasing need for economical, reliable, and rapid construction has made researchers question how these elements could be implemented in the building construction industry and to what extent it would be useful for it.

The traditional concrete construction industry has several challenges. One of them is high construction cost, which is directly related to the construction methods used for that specific project. The current concrete construction method involves the use of conventional formwork and scaffolding. Formworks are temporary molds that sustain the self-weight and fluid pressure of wet concrete. Scaffolding is typically used to provide access to the structure under construction. Even though these conventional methods are widely known and used by the majority of construction projects, the process of placing and erecting conventional formworks and scaffolding is time-consuming, which results in an increased construction cost. Several research shows that formwork costs are significant, accounting for up to 80% of overall concrete construction expenses. [1]

Another challenge is the remarkable amount of wastage generated during the construction. The use of formwork is the main source of the problem, since most of them are being discharged, which creates a cumulative construction waste in the industry. Another source of construction waste problem is generated by wasting materials on the

construction site due to human errors such as the lack of quality control, handling mistakes, and off-cut wastage. [2] This problem not only results in other time-consuming processes such as waste management but also creates serious issues with sustainability.

Moreover, current concrete construction involves serious time-consuming processes, which result in a slow speed of construction. Typical construction and manufacturing steps such as material preparation, transportation, and in-situ manufacturing require time. Moreover, labor errors often create problems that cause delays, which result in longer construction time.

Safety-related problems are another challenge of the current construction industry. Traditional construction methods have major safety issues which result in serious injuries and even construction deaths. The Occupational Safety and Health Administration (OSHA) has stated that more than 100 construction employees die on the job every week in the US. According to the statistics, construction accounting for nearly 20% of worker fatalities in the private sector, accounting for one out of every five worker deaths across all industries for the year. [1]

Last but not least, the conventional method of casting concrete using formwork limits the geometrical freedom of the structural elements. This problem not only creates an impediment for the creativity of the architects but also limits the use of curvilinear structural elements that can be more efficient than rectilinear shapes in various applications.

The additive manufacturing methods used in the robotic construction field, such as 3 Dimensional (3D) concrete printing, provide numerous benefits, including improved

safety, quality, and productivity. Moreover, it holds a great advantage for the construction of structural elements that are difficult to construct by conventional methods. The 3D-printing method is also flexible enough to create a variety of bridge elements, including cap beam shells [3,4] and column shells [5,6]. These advantages carry a huge potential for solving the aforementioned challenges.

Even though robotic construction technique offers great potential for the construction industry, there are challenges coming with this new technology such as its incompatibility with contemporary design and construction processes, the scarcity of customized structure components and connections for 3D printing, and the restriction of materials that can be used in automated construction. This research utilizes the development of Ultra-High Performance Concrete (UHPC) to achieve a high-performance cementitious material that can be used for automated construction and 3D printing purposes. [20]

1.2. Objectives

The aim of this thesis was to develop a 3D printable UHPC mixture using the local materials in Florida, USA. Conducting various experiments to evaluate the material properties of the developed mixes was one of the main objectives of this research.

1.3. Hypothesis

The 3D printing performance of the UHPC mixes is dependent on the properties such as buildability, extrudability, workability, open time, and mechanical features. As buildability, extrudability, workability, open time and mechanical strength increase, the

3D printing performance of the UHPC mix also increases. These properties can be manipulated by changing the volume percentage values of the mix components.

1.4. UHPC Properties

The term "Ultra-High Performance Concrete" (UHPC) refers to a new type of cementitious material that has recently been used for strengthening and repair of structures due to its superior properties such as advanced mechanical strength, durability, and long-term stability. Furthermore, the UHPC's ultra-high compressive strength allows for the creation of complicated volumes with narrow cross-sections, making it ideal for 3D printing. UHPC typically is composed of Portland cement, fine sand, supplementary cementitious materials, water, high-range water-reducing admixture (HRWR), and steel fibers. The steel fibers used in UHPC are cylindrical and nondeformable, with a length of 0.5 inches and a diameter of 0.008 inches. The volume of the steel fibers varies between 2% and 4% of the total volume.

The compressive strength of regular concrete ranges from 2.5 ksi to 4 ksi whereas UHPC has a compressive strength of more than 22 ksi. This shows that the UHPC has more than 5 times the compressive strength of the regular concrete. Furthermore, the UHPC has a tensile strength of more than 725 psi, which is nearly 2 times that of normal concrete. [21] It should be noted that Federal Highway Administration (FHWA) has recently reduced the compressive strength requirement for UHPC mixes from 22 ksi to 18 ksi based on yet to be published report.

Since UHPC has unique properties that are different from traditional cementitious materials, there will be some challenges during the adaptation process of this material to

a new system. Material-related challenges can be grouped under 5 categories as extrudability, workability, buildability, open time, and mechanical properties. [20]

1.4.1. Extrudability

Extrudability in 3D-printed cementitious materials is described as the capability of the fresh mixture to flow through the printing nozzle as a continuous filament without any damage. [7] A smooth flow of material in pumping hoses is one of the most important requirements for extrudability, which is called excellent flowability. Flowability, on the other hand, cannot ensure the desired extrusion through nozzles on its own. Hoses' dimensions and geometry may not always be consistent with the dimensions and geometry of the printing nozzles. As a result, if not designed appropriately, the difference in the cross-section between the pumping hose and the printing nozzle can create a blockage problem.

1.4.2. Workability

It is essential to know the definition of workability in order to understand the effect of workability on 3D-printed cementitious materials however, there has been a disagreement about the definition of workability. According to American Concrete Institute (ACI) Standard 116R-90 (ACI 1990b), workability is described as the quality of fresh concrete or mortar that controls the ease and uniformity with which it may be mixed, placed, consolidated, and finished. [8] The property of workability, as defined by ASTM C 125-93, is the work required to shape an amount of fresh concrete with minimal loss of homogeneity. [9] Workability (or, more accurately, printability) is the factor that governs the printing ability of a cementitious mixture. It's a hybrid quality made

consisting of at least four main elements, as listed above such as extrudability, flowability, buildability, and open time. [7]

1.4.3. Open Time

In the traditional concrete pouring method, open time is described as the time when the workability of fresh concrete is at a level that enables it to be poured. In other words, open time refers to the period between the inceptive contact of dry mix with water and the moment when the material is poured. [7] Since the printed concrete is not poured in one go as in the conventional method, establishing the open time criterion in the 3D printing process is different. The inceptive and final setting times are more representative of the latter, but they are of little use in concrete printing. As a result, open time measurement provides a better depiction of the actual differences in workability over time.

The end of open time is determined to occur when the shear strength of the material increases by 0.044 psi from its original shear strength. As the shear strength increases, workability decreases which creates growing difficulties in printing a filament of good quality [7] Therefore, the shear vane was used to determine the open time by measuring the workability of fresh concrete every 15 minutes.

1.4.4. Buildability

Buildability can be defined as the printed materials' resistance to deformation under load. In order to achieve the high geometric accuracy of 3D printed elements and prevent the collapse of printed structures, materials must have sufficient buildability

which will assure them to be strong enough after extrusion to support their own weight as well as the weight of the top layers. Insufficient buildability leads to one of the biggest problems of the additive manufacturing process which is the deformation of the printed filaments in the vertical and horizontal direction. The geometry of the printed component is significantly altered as a result of this problem. [7]

Hydrostatic pressure is the pressure applied by a fluid at equilibrium due to gravity at a specific position inside the fluid. Hydrostatic pressure rises in proportion to depth measured from the surface due to the rising weight of fluid exerting downward force from above. Even though this concept has been mostly seen as a governing factor while designing fluids and flowable mixes in conventional construction, it has a key role in the additive manufacturing process as well. The hydrostatic pressure rises with the height of the structure, and the layers compress under self-weight. The distance between the nozzle and the working surface grows as a result of maintaining a consistent layer height during printing, altering the shape of the printed layer, and potentially compromising layer adhesion. [10]

This effect becomes more prominent when the gap between the working surface and the nozzle widens, forcing the printed specimen to shift as it is extruded, eventually causing the buckling of the structure which leads to collapse. Figure 1-1 presents an empirical buildability test geometry developed by Buswell et al. In this study, researchers aimed to test the stability of the structure by varying the number of contiguous filaments per layer. This test can be used to determine the relationship between the number of contiguous filaments and the number of stacked layers. [10]

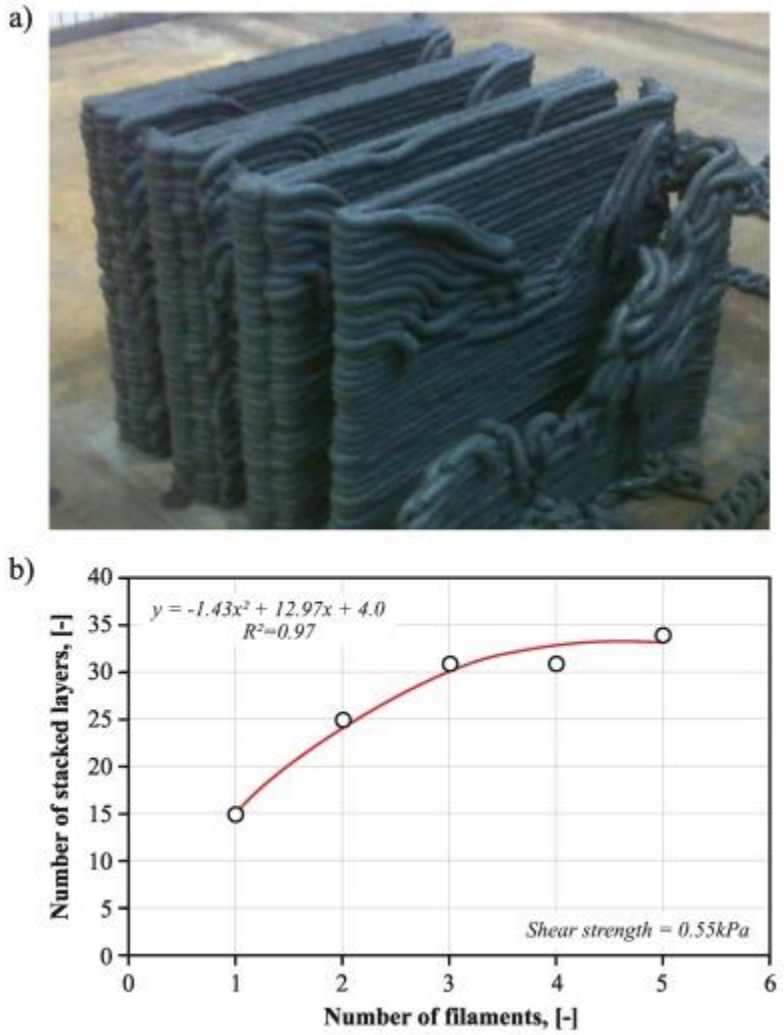

Figure 1-1. The buildability test designed by Buswell et al. in which a) the number of adjoining filaments per layer is altered to evaluate stability and b) the relationship between the number of stacked layers and the number of contiguous filaments was determined. [10]

1.4.5. Mechanical Properties

Mechanical performance of UHPC can be evaluated from properties that include, compressive strength, tensile strength, flexural strength, shrinkage and creep, porosity, density, and modulus of elasticity. Even though many modern autonomous construction techniques, such as 3D concrete printing, rely entirely on the adhesive (tensile) strength

along the interface area, traditional concrete design standards make it impossible to use this tensile strength when calculating structural resistances. This tension is exacerbated by the fact that additively made components by their nature have a non-homogeneous internal structure due to the layering of filaments. On a macroscale, the interfaces cause the anisotropic behavior of hardened printed concrete, which must be taken into account while designing printed members. Furthermore, the tensile strength and mechanical properties of interface regions are dependent on the amount of time that has passed after the application of two subsequent semi-fresh concrete layers. [22]

The compressive strength is typically controlled by the water-to-cement ratio (W/C) and water-to-binder ratio (W/B). For 3D printing purposes, the compressive strength of the UHPC is reliant upon the test direction. Cube, cylinder, or prism specimens can be utilized to evaluate the compressive strength of the material. In this research, cubical and cylindrical specimens were used.

1.5. Literature Review

There are several studies that have been conducted on the additive manufacturing process with cementitious materials. These studies hold great importance while understanding the criteria that need to be considered while developing a cementitious material for 3D printing.

Six cementitious materials have been designed by a team of researchers from Nanyang Technological University, Singapore to enable 3D printing utilizing a group of robots while fulfilling the rheological printing needs of yield stresses as well as the velocity. [11] One of these developed materials consists of fiber reinforced concrete mix

design whereas the other mixes consist of the ordinary concrete mix with its specifically designed properties for autonomous construction purposes.

Concrete comprised mostly of hydraulic cement, aggregates, and discrete reinforcing fibers is known as fiber-reinforced concrete (FRC). Mortars, normally proportioned mixes, or mixtures specifically designed for a particular application can all be used as concrete bases. Steel, glass, and organic polymers (synthetic fibers) have all been used to create fibers appropriate for reinforcing concrete. Natural asbestos fibers, as well as vegetable fibers like sisal and jute, are also used for reinforcement purposes. One of the most significant advantages of utilizing the fibers as a method of reinforcement is the advancements in long-term serviceability.[8]

Fiber-reinforced concrete mix developed by Zhang et al. consists of the ingredients such as Portland cement, sand, silica fume, water, HRWR, and steel fibers. All the other mixtures followed a conventional concrete mix design with variations in the sand component. Through modifying the type and the percentage of the sand, they have generated different mixes which were analyzed to achieve an optimal mix design for 3D printing purposes. Finally, researchers have performed a series of tests including not only the strength tests but also printability and extrudability experiments. Researchers have managed to physically print a structure with dimensions of 6.1 feet x 1.5 feet x 0.42 feet (length, width, height) using one of the developed mixes. Figure 1-2 presents the printed specimen after 10 days of curing. [11]

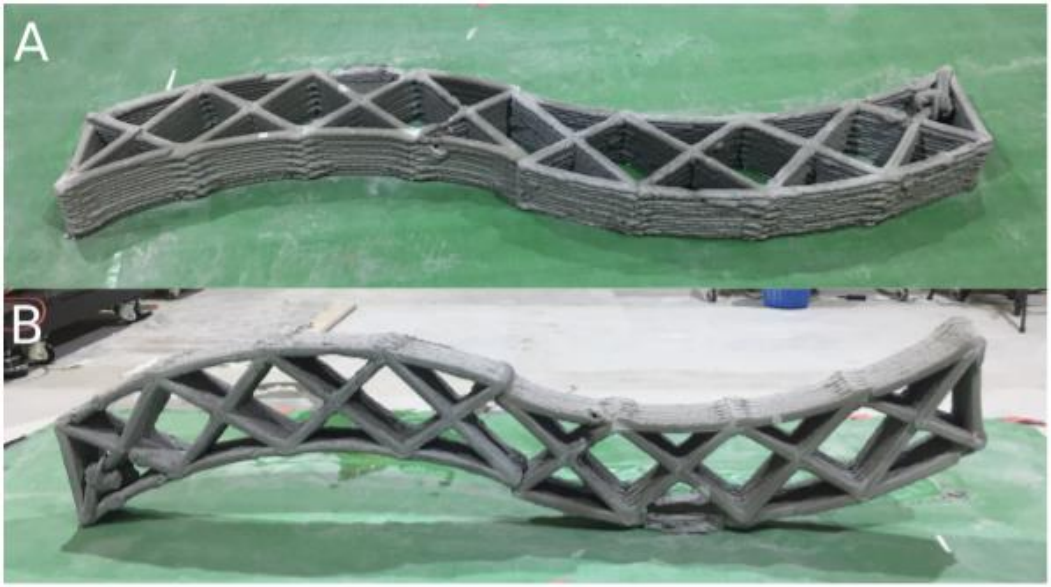

Figure 1-2. Printed specimen by Zhang et al. after 10 days of curing. [11]

Another article from the same journal was published with the studies conducted by Liu et al. who have worked on the topics related to the material rheological properties such as static yield stress (i.e., the critical stresses for the printed material that enable steady-state flow) and dynamic yield stress. [12]

Researchers have developed a mix design using typical components such as Portland Cement, silica fume, sieved sand, fly ash, water, and HRWR. The mixture design model of Design of Experiments (DoE) was utilized in the study to analyze the impacts of the input variables such as the volume fraction of the ingredients on the response which are directly related to the rheological properties. The acceptable components of the cementitious material were determined using optimization techniques. Researchers have stated several outcomes from the study which were informative while determining the effects of each component on the mix design. Moreover, the team has managed to

successfully print a spiral structure of 25 layers with 0.59-inch thickness for each layer using the optimized mix developed. Figure 1-3 presents the images from the successfully printed spiral structure.

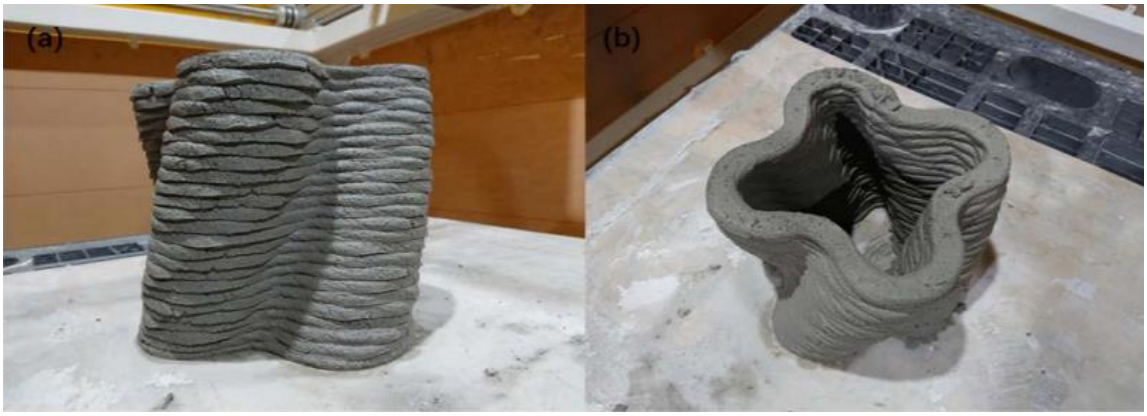

Figure 1-3. Successful printing of spiral structure with the material developed by Liu et al. (a) side view, (b) top view. [12]

Tay et al. [13] created a mix design by examining the bond strength in between the printed layers as well as the effect of the time difference between them. The extrusion-based 3D concrete printing has a layer-wise manufacturing method. Therefore, the printing time gap between layers must be considered carefully since it has a significant impact on the bond strength between the filaments.

The researchers created a mix design using ordinary Portland cement, silica fume, fly ash, and river sand. Since the primary purpose of this study was to improve the inter-bonding layer and introducing additives may make this process more complicated, no additives were used in this research. Several test setups were created to measure the rheological properties of the mix as well as the tensile bond strength between the two layers.

It is stated in the article that the initial layer's high modulus inhibited good contact and mix at the interface. It was also one of the outcomes that the increased time gap causes voids to form at the interface area, which weakens the bond strength in a logarithmic pattern. Figure 1-4 presents the comparison between samples printed at different time-gap values. It is possible to see from the figure that over larger time gaps, distortion appears across the printed layer at the interface surface. The weight of the subsequent layer, as well as pressures encountered in the duration of the printing process, are some of the reasons that cause the material at the interface to distort. If the time gap of the material is short, this disruption is beneficial for the interaction and bonding of the materials at the interface. However, as the time gap increases, it gets harder for the material at the interface to interact. This is the reason behind the occurrence of the voids at the bond interface and eventually the deformation of the printed material. [13]

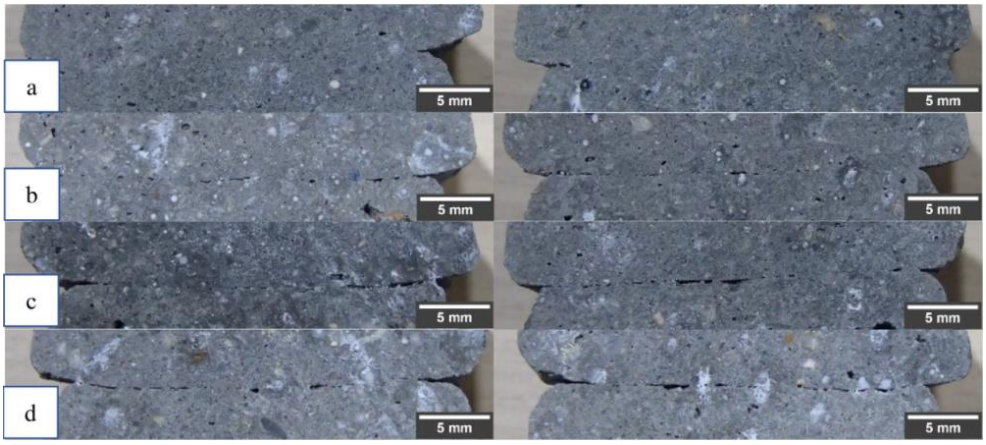

Figure 1-4. Samples printed by Tay et al. at a time gap of (a) 1 minute, (b) 5 minutes, (c) 10 minutes and (d) 20 minutes. [13]

Kazemian et al. [14] designed four fiber reinforced cementitious mixes that include sand, cement, water, HRWR, and polypropylene fiber. A viscosity modifying additive

(VMA) for anti-washout concrete was also utilized to enhance the plastic viscosity and cohesiveness of printing mixes. In this study, the effects of nano-clay, silica fume, and fiber inclusion were all investigated through the developed mixes. A linear concrete printing robot was built to make laboratory testing easier. Figure 1-5 presents the linear concrete printing machine used in the research.

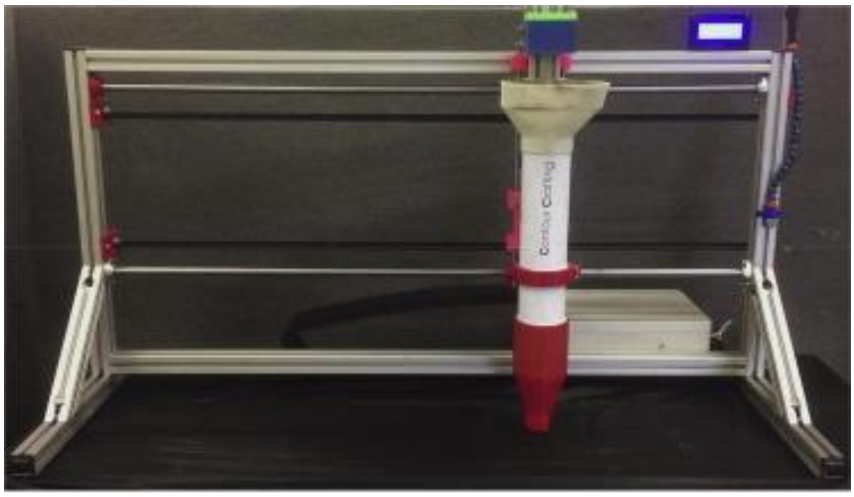

Figure 1-5. Linear concrete printing machine constructed and used by Kazemian et al. [14]

Several test setups were used in their research to analyze the different factors determining the 3D printing process of the designed mixture such as printing quality, shape stability, and printability window which will be referred to as the “open time” in the following chapters of this thesis. In order to examine and adjust the three recommended workability aspects of a printing combination, researchers used an iterative laboratory testing approach. Experiments found that the addition of silica fume and Nano-clay to a fresh printing mixture improves shape stability, whereas adding

polypropylene fiber creates a slight effect on the improvement of the shape stability only. [14]

Le et al. [15] also introduced a series of mixes with varying sand/dry mix ratios. The dry mix in this research was determined to be consist of cement, sand, fly ash, and silica fume. Buildability and extrudability, which are correlated with open time and workability, were identified to be the most critical fresh qualities in this study. Definitions and test methods are presented to make a comparison between mixes by evaluating these fresh properties. The best mix was determined to be the one with a 3:2 sand/binder ratio, containing 70% cement, 10% silica fume, 20% fly ash, and polypropylene fibers. The developed material was tested by the full-scale manufacture of a bench component. Figure 1-6 shows the bench component during the printing process.

Figure 1-6. Bench structure designed by Le et al. during the printing process. [15]

After multiple studies with various mix combinations, Paul et al. [16] produced three ideal mixes. These mixes were created to investigate the materials' fresh and mechanical properties in reference to the printing direction. After the layer was placed, the final mix design was determined considering flowability, pumpability, and shape retention abilities. The workability of the fresh materials was assessed using flowability and rheology tests.

In this research, multiple tests were used to analyze the fresh and mechanical properties of the cementitious mixtures. The Bingham model for non-Newtonian materials was utilized to determine the expected shear stress and plastic viscosity of the mixtures. The rheology of the developed mixes was measured using a rheometer. The open time was determined by observing the differences in the workability of the mixture after equal time intervals. The flexural and compressive strength tests were performed to analyze the mechanical properties.

It is mentioned in the article that in additive manufacturing, printing parameters such as nozzle size, printed objects, etc. control the mechanical characteristics of the material, which must be considered while designing any structure for 3D printing. To evaluate this concept, researchers have printed rectangular objects using the developed mix and collected specimens from different directions for testing. Figure 1-7 presents the objects printed for this research with different printing directions. The ultimate compressive strengths of the mixes were tested to be in the range of 5.2 ksi to 8.2 ksi. Researchers have reached the conclusion that the specimens obtained from the printing direction have higher strength compared to the specimens obtained from the other directions after testing for 28 days strength. [16]

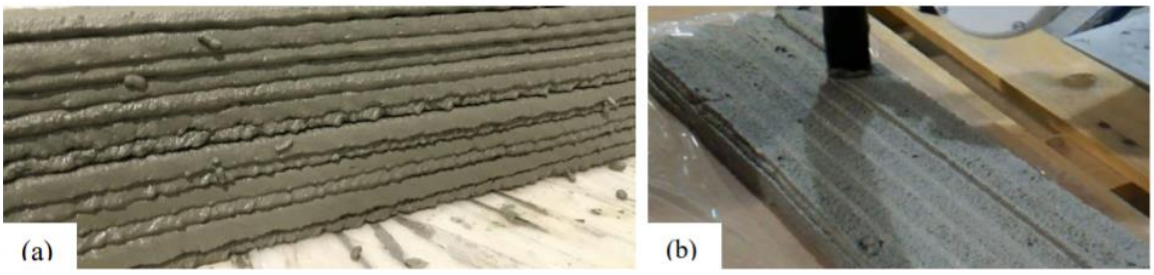

Figure 1-7. Printed objects created by Paul et al., a) side view and b) top view [16]

Weng et al. [17] developed six different cementitious materials which consist of natural river sand, Portland cement, silica fume, fly ash, water, and HRWR admixture. These mixes were developed using five different types of sand and five different gradation processes. To evaluate the fresh performance of all combinations, rheological experiments were undertaken, and printing tests for buildability were conducted using a gantry printer. Figure 1-8 presents the gantry printed structure. Researchers have also studied the density and mechanical properties (compressive and flexural properties) of the material.

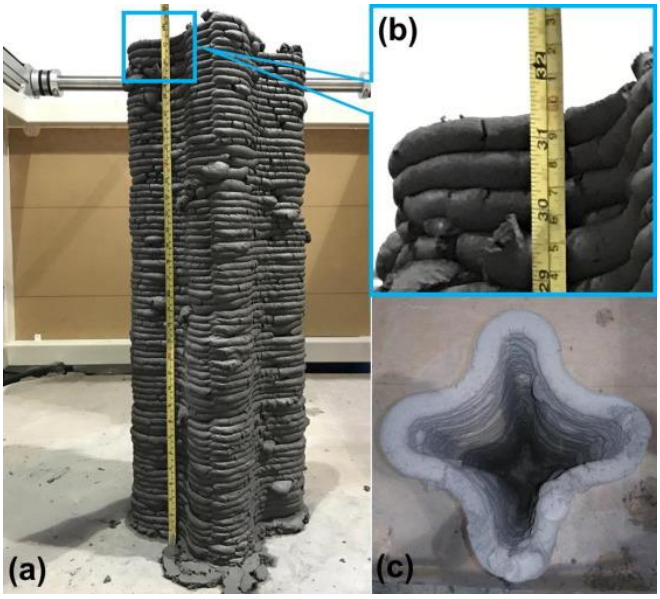

Figure 1-8. Gantry printed structure developed by Weng et al.: (a) final structure; (b) height and layer thickness and (c) top view of the printed structure. [17]

In conclusion, the researchers have reached an outcome as a result of the rheological tests that without noticeable deformation, the mixture with the highest yield stresses and lowest plastic viscosity can reach up to 15.7 inches (40 layers). It has also been stated that it is possible to use the Fuller Thompson approach and the Marson-Percy model as design guides to develop materials in a way that will allow them to reach to the desired mechanical and rheological characteristics for 3D printing. This design guide may be utilized to create a good balance of yield stress and plastic viscosity since the increased yield stresses are needed to ensure the buildability and decreased plastic viscosity is needed for a good pumping performance. [17]

Arunothayan et al. [18] developed a non-proprietary 3D-printable mixture utilizing VMA in addition to HRWR admixture. Researchers have computed the mixing

proportions of the UHPC mix by optimizing the particle packing density qualities of the dry materials utilizing the modified Andreasen and Anderson (modified A&A) model.

To determine the optimal HRWR and VMA percentages that will allow the designed mixture to fulfill the extrudability, workability, and buildability criteria, several trials of the UHPC mixes were performed. Until the flow table was dropped, the spread diameters of the UHPC mixes were almost equal to the bottom diameter of the brass cone employed in this experiment, showing that the fresh mixtures had approximately no flowability, which was defined to be ideal for extrusion-based 3DCP. [18]

The designed mix was tested by printing five individual layers, with a length of minimum 10 inches. No tearing, blockage, bleeding, or segregation was observed throughout the experiment. This means that the created UHPC mixture has met the extrudability requirement. The specimens were tested under increasing vertical load to analyze their shape-retention-ability (SRA). Finally, a large-scale structure with a curvilinear geometry was printed using the designed mix. Figure 1-9 shows the large-scale 3D printing process of the curvilinear bench as well as the pictures showing the final state of the structure.

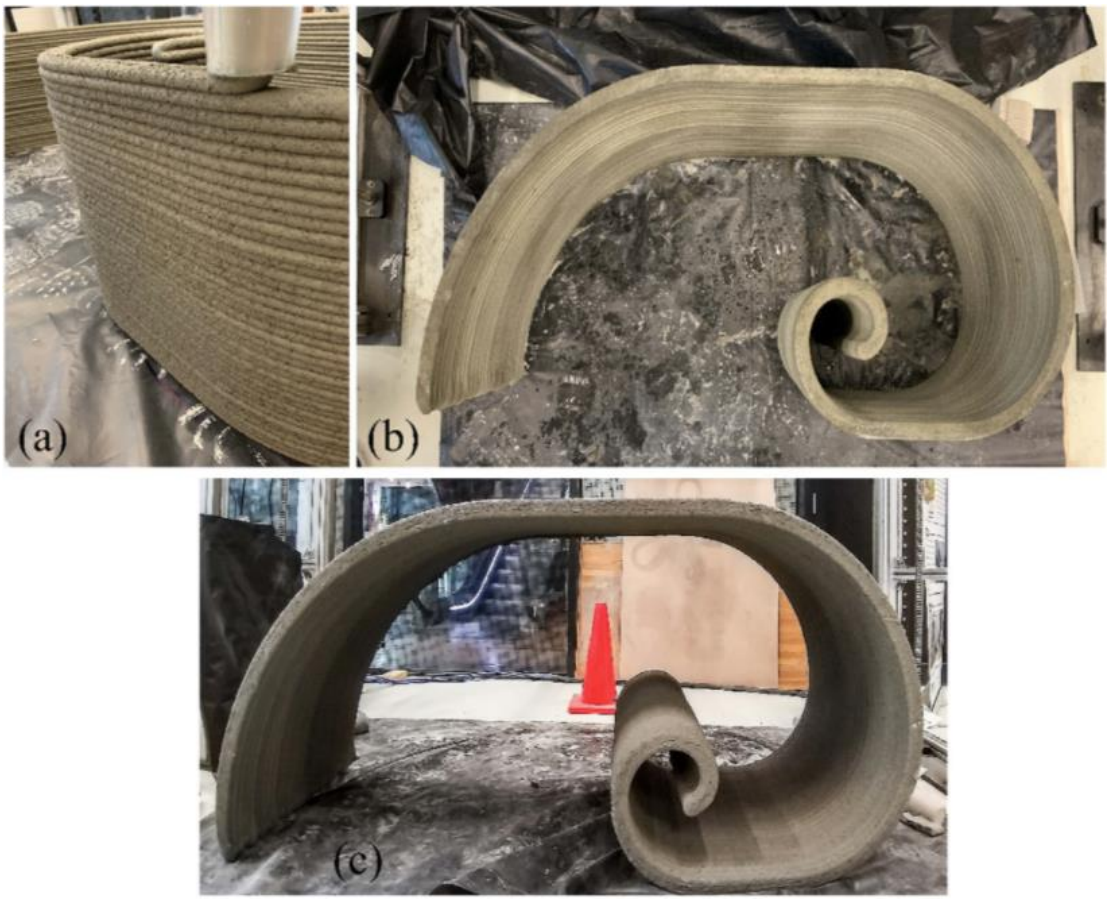

Figure 1-9. 3D printing of a curvilinear bench using the mixture developed by Arunothayan et al. (a) the printing process; (b) top view; (c) front view. [18]

It should be noted that the mix developed by Arunothayan et al. was used as the base design for this thesis and adjustments in the HRWR content were made in order to modify the mix to achieve target metrics. The further details of the adjustments as well as the mix design proportions will be shown in the Material Development section of this thesis.

Zhu et al. [19] created mixtures with ultra-high tensile ductility for additive manufacturing purposes. Hydroxypropyl methylcellulose (HPMC) was utilized in this research. In this study, the fresh and hardened characteristics of 3D printable engineered

cementitious composites reinforced with high-density polyethylene (PE-ECCs) were investigated.

The produced 3D printed PE-ECCs exhibit a strong strain-hardening behavior and ultra-high tensile ductility, depending on the fiber composition. The test results have shown that these mixes have a compressive strength of 6.8 to 7.4 ksi, a flexural strength of 1.9–2.8 ksi, a uniaxial tensile strength of 0.826 ksi, and a tensile strain capacity of 3.57–11.43 percent.

The study found that as the volume percent of fibers increases, the strain energy, tensile strain capacity, and the number of cracks all increase remarkably. The 3D concrete printing approach enhanced the fiber alignment by allowing the fibers to be more parallel to the direction of the force, as opposed to arbitrary dispersion of the classic mold-casting process. Furthermore, the scanning electron microscopy (SEM) examination revealed that the 3D printing method enhanced the microstructure of the developed mix, resulting in pores that were more homogeneous in terms of the distribution as well as the size. These are the reasons behind the improved tensile performance of the specimens. Figure 1-10 presents the differences between the SEM examination results of the developed mix using the mold cast specimen and the 3D printed specimen.

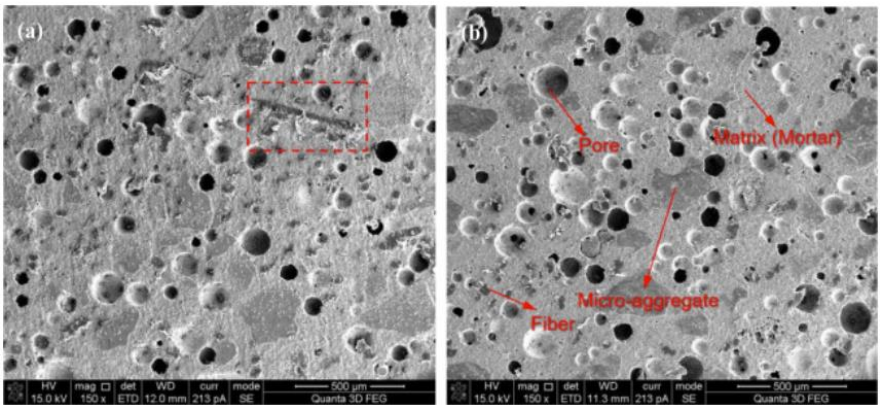

Figure 1-10. The SEM study developed by Zhu et al.: (a) Mold cast specimen; (b) 3D printed specimen. [19]

3D printed samples had somewhat higher flexural strength than conventionally mold-cast samples. This is due to the fibers' enhanced orientation in the 3D printed samples. The 3D-printed specimens, on the other hand, had a slightly lower compressive strength than the mold-cast specimens. This could be due to the fact that the 3D printing process creates pores between the printed layers that generate weaker zones through the sample.

Mixes containing 2% (by volume) PE fibers had 47% greater flexural strength than mixes containing 1% (by volume) fibers. However, as the volume percentage of the fibers increases from 1% to 2%, the effect of fiber content on compressive strength decreases. This conclusion is valid for both mold-cast and 3D printed specimens.

Yang et al. [23] developed a novel UHPC mix for 3D printing purposes. Compressive, flexural, uniaxial tensile, and splitting tensile tests were utilized to explore the influence of the fiber type, fiber volume fraction, and printing direction on the mechanical and anisotropic characteristics of the mix. As a result of these experiments, the researchers found that under the same printing parameters, the mixture developed

with 6 mm steel fibers is more applicable for construction compared to the mixture prepared with 10 mm steel fibers.

The researchers have reached the highest flexural strength was 6.7 ksi in the printing direction. According to the research, the flexural and splitting tensile failures of the specimen may be brittle or ductile depending on the testing directions, therefore it is crucial to adjust the printing method in order to meet the diverse engineering needs. Figure 1-11 presents the comparison between flexural, splitting, and uniaxial tensile strength values for the mix with the fiber content of 1% in volume.

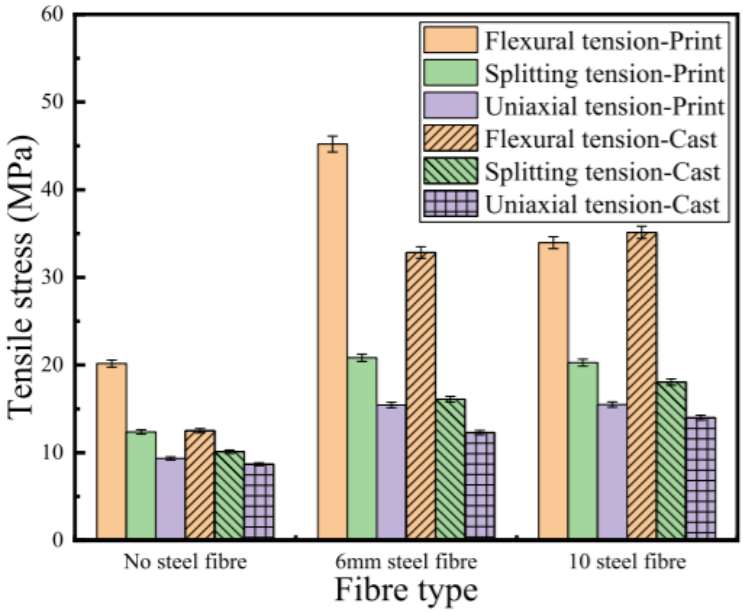

Figure 1-11. Comparison between the flexural, uniaxial and splitting tensile strength values. [23]

Table 1-1 was developed by Javed et al. [20] to demonstrate the different mix compositions proposed by the above-mentioned researchers for various cementitious materials that were developed for 3D printing purposes. It is possible to see from the

table that the highest strength achieved from the abovementioned studies was 18.19 ksi which was obtained by Arunothan et al. This mixture consists of cement, silica fume, sand, water, HRWR, VMA, and fiber content of 2% by volume.

Table 1-1 Variety of mix compositions by weight developed for 3D printing purposes. [20]

Mix no.	Reference	Cement	Fly ash	Silica fume	Sand	Water	HRWR (SP)	Fiber (lb/yd^3)	HPMC	VMA	f'c (ksi)
1	Zhang et al. (*13*)	0.288	0.135	0.027	0.360	0.189	0	0	0	0	na
2		0.196	0.196	0.294	0.201	0.113	✞	0	0	0	na
3	Liu et al. (*14*)	0.238	0.234	0.019	0.291	0.218	0	0	0	0	na
4	Tay et al. (*15*)	0.263	0.075	0.038	0.451	0.173	0	0	0	0	na
5	Kazemian et al. (*16*)	0.268	0	0	0.616	0.116	0.0005	0	0	0	6.48
6		0.243	0	0.027	0.611	0.117	0.0018	0	0	0	7.24
7		0.268	0	0	0.615	0.116	0.0006	2.02	0	0	6.54
8		0.268	0	0	0.615	0.116	0.0017	0	0	0	6.66
9	Le et al. (*5*)	0.164	0.047	0.023	0.701	0.065	0	0	0	0	na
10		0.194	0.055	0.028	0.646	0.077	0	0	0	0	na
11		0.223	0.064	0.032	0.592	0.089	0	0	0	0	na
12		0.251	0.072	0.036	0.538	0.094	0.01	2.02	0	0	15.95
13		0.280	0.080	0.040	0.488	0.112	0	0	0	0	na
14	Paul et al. (*12*)	0.131	0.126	0.066	0.548	0.129	0	0	0	0	7.54
15		0.130	0.125	0.065	0.545	0.128	0	22.75	0	0	6.96
16	Weng et al. (*17*)	0.345	0.345	0.035	0.172	0.103	✠	0	0	0	7.21
17	Arunothayan et al. (*18*)	0.321	0	0.138	0.459	0.073	0.0069	***	0	0.0014	18.19
18	Zhu et al. (*19*)	0.43	0.57	0	0.405	0.28	✧	***	0.001	0	8.09
19		0.43	0.57	0	0.405	0.28	✧	**	0.001	0	7.66
20		0.43	0.57	0	0.405	0.28	✧	*	0.001	0	7.43

Note: ksi = kips per square inch; HRWR = high range water reducer; SP = superplasticizer; HPMC = hydroxypropyl methylcellulose; VMA = viscosity modifying agent; na = not applicable.

*1% is added by volume.

**1.5% is added by volume.

***2% is added by volume.

✞ 2.36 lb/yd^3.

✠ 0.58 lb/yd^3.

✧ 0.012 lb/yd^3.

2. MATERIAL DEVELOPMENT

In this research, the mix developed by Arunothayan et al. [18] was used with the same proportions as the base mix. This mix was adapted by modifying the amount of HRWR and replacing the contents with local materials in Florida. Table 2-1 presents the mixture proportions of UHPC material developed by Arunothayan et al. [18].

Table 2-1 Mixture proportions of the printable UHPFRC developed by Arunothayan et al. [18].

Binder		Silica sand			Water	HRWRA	VMA	Fiber
Cement	Silica fume	Fine	Medium	Coarse				
0.7	0.3	0.4	0.3	0.3	0.16	0.015	0.003	2%

Note: All numbers are mass ratios of the binder weight, except the fiber content (volume fraction).

The binder of the UHPC mix consists of Portland Cement (Type II) and silica fume. Three types of sieved sand based on their particle size distributions have been utilized. The fine, medium and coarse sands have particle sizes of 0.250 mm, 0.425 mm and 0.850 mm respectively. To modify the workability, a high-range water-reducing admixture (HRWR) was utilized. Viscosity modifying admixture (VMA) was used to adjust the rheological properties of the mix for 3D printing purposes. Cylindrical, non-deformable steel fibers with a length of 0.5 inches and a diameter of 0.008 inches have been used at a volume fraction of 2%.

Several experiments of the UHPC matrix and composite were conducted to fulfill the buildability, extrudability, and workability parameters. Table 2-2 shows the mixing percentages of the designed 3D-printable UHPC material.

Table 2-2 Mixture proportions of the printable UHPC.

Material	Amount (lb/ yd^3)	Percent by Weight
Portland Cement	1233	29.8
Silica Fume	528	12.8
Masonry Sand	1761	42.6
Water	282	6.8
HRWR	71	1.7
VMA	5	0.1
Steel Fibers	258	6.2

Even though increasing flowability results in decreased buildability, which makes this approach not preferable for 3D printing purposes, low flowability also may cause serious problems for the 3D printing system such as blockage and pumpability issues. Therefore, in order to create a guideline for future 3D printing applications, several variations of the mix were developed with different flowability behaviors. The matrix mix was re-designed with different percentages of HRWR to increase the flowability and decrease buildability to a point where both flowability and buildability works for 3D printing purposes. Table 2-3 presents the different mixtures created by modifying the amount of HRWR.

Table 2-3 UHPC mix variations developed by changing the amount of HRWR

	Weight (lbs) per CY						
MIX ID	Reg. Cement	Silica Fume	Masonry Sand	Water	HRWR	VMA	W/B
A	1275	546	1821	291	49	5	0.16
A-101	1266	543	1808	289	61	5	0.16
A-102	1257	539	1796	287	73	5	0.16
A-103	1241	532	1772	284	96	5	0.16

It should be noted that required adjustments were made in order to maintain the proportions between each raw material while increasing the amount of HRWR in the UHPC mixture. Water-to-binder (W/B) and water-to-cement (W/C) ratios were kept the same.

In order to see the effect of VMA on flowability, buildability, and mechanical properties of the mix, two variations were created by eliminating the VMA. Table 2-4 shows the proportions of the mix without VMA. Again, proportions between each material as well as the water-to-binder (W/B) and water-to-cement (W/C) ratios remained the same.

Table 2-4 UHPC mix variations developed by changing the amount of HRWR and eliminating VMA.

	Weight per CY						
MIX ID	Reg. Cement	Silica Fume	Masonry Sand	Water	HRWR	VMA	W/B
A	1275	546	1821	291	49	5	0.16
A-201	1245	543	1778	284	96	0	0.16
A-202	1228	526	1755	281	118	0	0.16

Steel fibers are utilized in 3D printable cementitious materials to improve structural strength, minimize steel reinforcing requirements, reduce fracture widths, and precisely control crack widths, resulting in improved durability. Besides these factors, reinforcing fiber has an influence on material flow behavior.

As flowability decreases, the buildability increases, improving the quality of printed layers and reducing the possibility of vertical and horizontal deformation of deposited layers. Even though implementing steel fibers to the developed mixes has a great potential to create a suitable reinforcement approach for 3D-printable cementitious materials, it may result in problems related to flowability. Steel fibers decrease the flowability which might create a blockage problem in the cross-section between the pumping hose and the printing nozzle, which may potentially lead to deformations in the printing robot. Therefore, it is essential to make revisions in the printing material as well as the mixing process to make it suitable for the implementation of steel fibers.

In this research, after many experiments, Mix A-102 was determined to be the optimum mix for the development of the composite material which includes the steel fiber component. Then, Mix A-S-102 was designed using the same material proportions and inducing the steel fibers. Table 2-5 presents the detailed material proportions between the two mixes. Again, revisions were made to ensure that proportions between each material as well as the water-to-binder (W/B) and water-to-cement (W/C) ratios remain the same.

Table 2-5 UHPC mix variations with and without steel fibers.

	Weight per CY						
MIX ID	Reg. Cement	Silica Fume	Masonry Sand	Water	Steel F.	HRWR	VMA
A-102	1257	539	1796	287	0	73	5
A-S-102	1233	528	1761	282	258	71	5

3. EXPERIMENTAL METHODS

3.1. Mixing

A small bread mixer with 0.15 cubic feet capacity was used in this research. First of all, the dry components (binder and sand) were mixed together for 5 minutes. After that, approximately 75% of the water was added to the dry material and mixed for 5 more minutes. HRWR was mixed with the remaining water and gradually added to the mix. Another 10-15 minutes of mixing was required to achieve suitable rheology. Then, steel fibers were added to the mixer gradually and mixed for 5 minutes. Lastly, VMA was added and mixed for 5 more minutes. The total mixing time was approximately 30 minutes.

3.2. Printing and Casting

In this research, two types of specimens were used to conduct compressive strength tests. 3 inch x 6 inch cylindrical molds and 2 inch x 2 inch cubical molds were used to cast specimens. Cylindrical specimens were used for perpendicular strength tests. Cubical specimens were cast in 2 stages in order simulate the interface area between two layers.

First, half the height of the specimen (1 inch) was cast. This phase demonstrated the first layer of printing. Then, the second half of the specimen was cast after 10 minutes which acts as the second layer of the printing process. With this approach, an interface area was created between the two layers. Finally, the specimens were tested in three orthogonal directions to analyze the differences between the strength of the specimens when the load is parallel and perpendicular to the printing direction. Figure 3-1 presents the cubical specimens as well as the orthogonal testing directions used.

Figure 3-1. Cubical specimens used for testing in three orthogonal directions.

A large-scale 3D printer is currently being developed by Florida International University for 3D concrete printing purposes. To demonstrate the printing process of the material and test the extrudability properties of the UHPC mix, a rectangular nozzle of 2 inch x 1 inch was manually used.

3.3. Curing and Grinding

After completing the casting process, specimens were cured in ambient conditions for 7 days, 14 days, and 28 days. Specimens were demolded right before testing. Two sides of cylindrical specimens were ground using a concrete grinder to achieve a smooth surface for compression tests. Then, the dimensions of the specimens were measured using a scale and a digital caliper.

3.4. Test Methods

Test methods can be categorized under two sections as the tests conducted on the fresh mixture and the tests related to the hardened properties of the mix.

3.4.1. Fresh Properties

Three different tests were conducted on the fresh properties of the developed UHPC mix. The workability performance of the fresh UHPC mix was analyzed using static flow tests in accordance with ASTM C1437 [9]. Fresh UHPC mix was poured into a conical brass mold. The mold was removed after one minute and the timer was set for another minute. The mixture flow was then measured in two orthogonal directions.

To measure the extrudability properties of the UHPC mix, a qualitative method was used. UHPC was manually printed using a rectangular nozzle of 2 inch (W) x 1 inch (H). Figure 3-2 presents the details of the nozzle geometry.

Figure 3-2. Rectangular printing nozzle of 2 inches by 1 inch.

The acceptance criterion for the extrudability test was to achieve 15 inch long continuous layers without observing any visual deformation on the printed layer. Also, a 90 degrees corner layer was printed to see the behavior of the developed material in curvilinear printing applications. The thickness of the layer was almost equal everywhere except for the parts where the test was paused to add more UHPC to the system to continue extruding.

To evaluate the buildability feature of the UHPC, the fresh mixture was filled into a cylindrical mold of 3 inch (D) x 3 inch (H). Then the mold was removed and

rectangular plates each weighing 0.82 pounds were gradually loaded on the fresh mix until a visual deformation has been observed. After each loading, a camera was used to record images of the fresh samples. It should be noted that several researchers have previously utilized this approach to assess the shape retention ability of fresh mixtures.

3.4.2. Hardened Properties

Specimens were tested for their compression strength using a concrete compression machine. Figure 3-3 presents a typical setup used for testing specimens for their compression strength. An average of 250 lbs/sec constant load control rate was applied to all specimens as per ASTM requirements. [9] Test results including total load applied on the specimen as well as the calculated compression strength and the average loading rate were recorded.

Figure 3-3. Typical compression test setup.

4. FINITE ELEMENT ANALYSIS

Finite element models have been generated using the ATENA software in order to achieve a further detailed analysis of the developed UHPC mixes and make a comparison between them by calculating the maximum number of layers that can be printed using the fresh properties of the developed mixes without failure.

In order to make this comparison, a cylindrical printing path with an outer diameter of 2 feet was generated. Each layer was determined to have 2 inches in width and 1-inch height. The finite element analysis was performed after the completion of each layer not only to observe the differences in deflection values but also to estimate the final printable layer before failure. Figure 4-1 presents the generated geometry for the finite element analysis as well as the layering system.

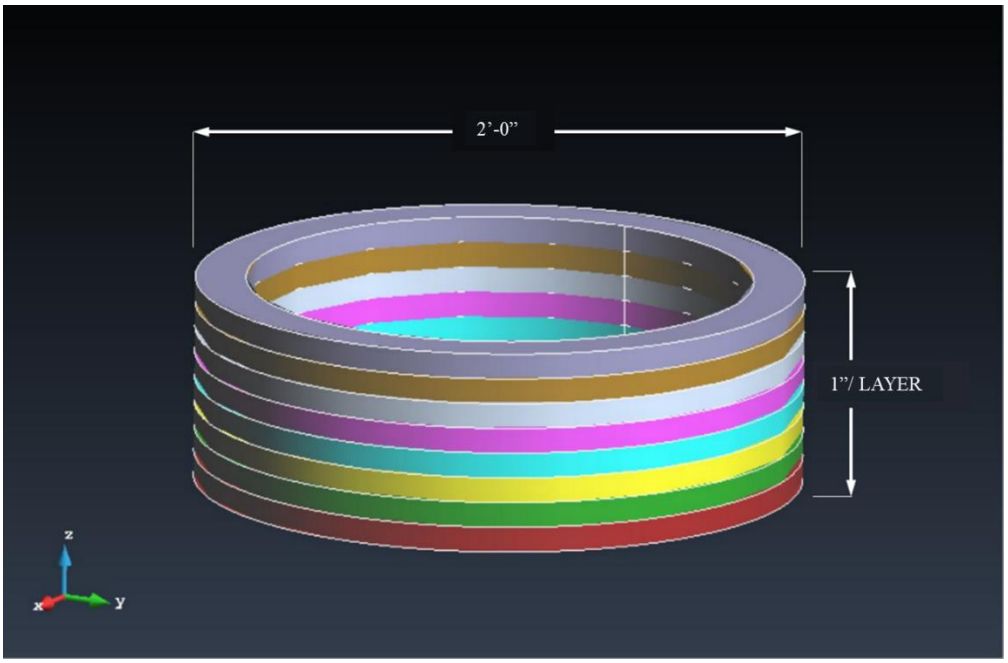

Figure 4-1. Finite element model layer geometry.

A 4-noded tetrahedral meshing was created on each layer in order to create finite elements and run the analysis with accuracy. With this meshing type, each triangle of the surface mesh is a side of one or two adjacent tetrahedrons. Figure 4-2 presents the meshing geometry of the generated model.

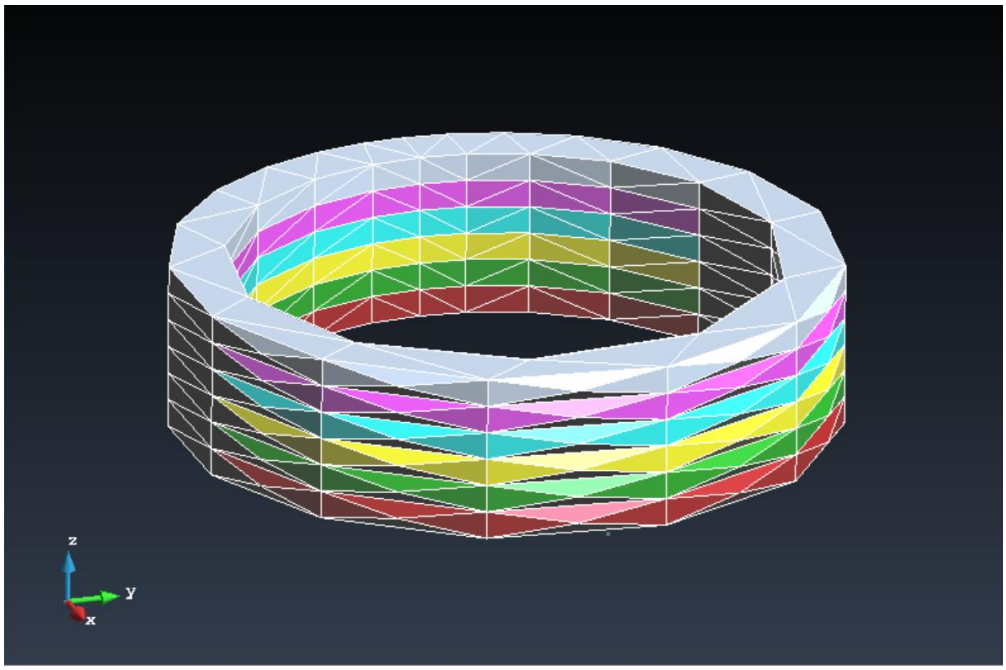

Figure 4-2. Meshing geometry of the generated model.

Material properties of the developed UHPC mixes were achieved using the experimental test results mentioned above and the numerical methods. Cervenka Consulting, the software development company that created ATENA software, has organized a webinar and published a paper in 2020 specifically on the topic of finite element analysis of the 3D printed concrete structures. [25] In this paper, researchers have used the article by Wolf et al. [26] as the base of their numerical calculations. Wolf et al. has studied the early age mechanical behavior of 3D printed concrete, which is a topic that is specifically important for 3D concrete printing applications. Since the

material is still in the fresh state during the 3D printing process, it is not possible to use hardened mechanical properties of the concrete while generating the finite element analysis. This article provides numerical methods that can be used while calculating the inputs that can be used for finite element analysis.

Wolf et al. tested the concrete specimens for their early age strength. During this study, it has been observed that the mechanical behavior of fresh concrete changes in the early age of 0 to 90 min. Researchers have also stated that in the beginning phase of the test, as the vertical displacement rises, the load increases almost linearly. However, after this initial phase, as deformations increase, the loading increment diminishes. After these observations, researchers have converted the load-displacement data into stress-strain diagrams. Figure 4-3 presents the stress-strain diagram of compression tests for concrete age t = 30 mins. The grey lines represent the individual test results whereas the solid black line represents the average stress-strain relationship.

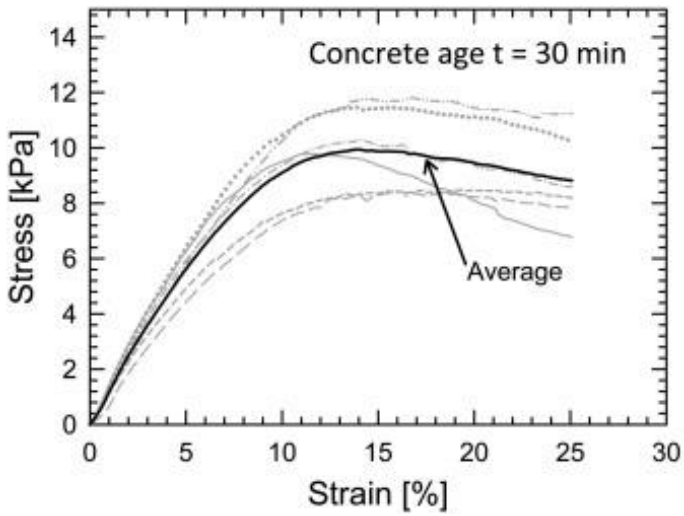

Figure 4-3. Stress-strain diagram of compression tests for concrete age t = 30 min. The grey lines indicate the individual tests results, the solid black line represents the average stress-strain relation. (1Kpa = 0.000145 ksi)

As an outcome of these studies, Wolf et al. has generated compressive strength development and Young's modulus development graphs. Figure 4-4 presents these graphs which has been used while calculating the compression strength gain of UHPC during the curing period.

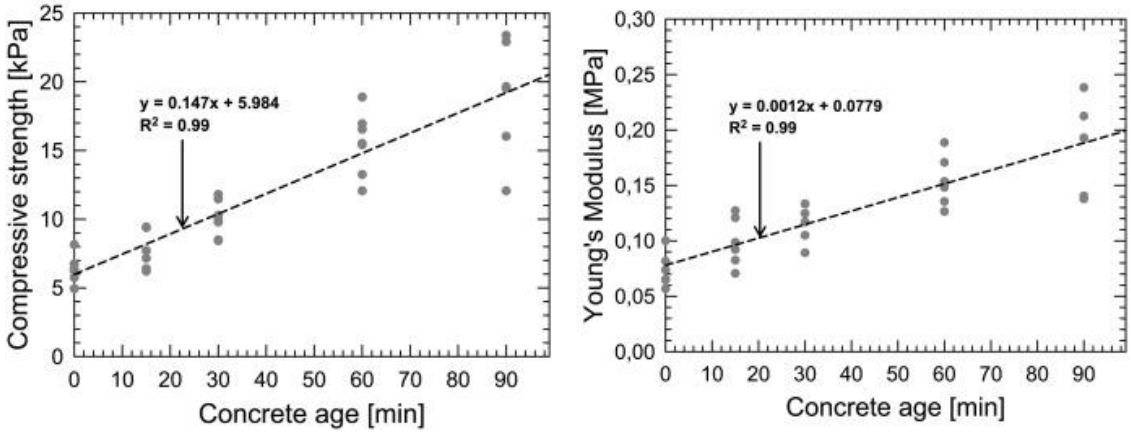

Figure 4-4. Compressive strength development (left) and Young's modulus development (right) up to 90 min derived from the compression tests by Wolf et al.

(1 kPa = 0.000145 ksi)

Researchers have developed a table that specifically shows the values of compressive strength, Young's modulus, and density derived from the uniaxial unconfined compression test. Table 4-1 presents the values of this table developed by Wolf et al.

Table 4-1. Compressive strength, Young's modulus and density derived from the uniaxial unconfined compression test, with average values μ, standard deviation σ, and relative standard deviation RSD. (1 kPa = 0.000145 ksi)

Concrete age [min]	Compressive strength σ_y [kPa]			Young's modulus E [MPa]			Density ρ [kg/m^3]		
	$\mu_{\sigma y}$	$\sigma_{\sigma y}$	RSD	μ_E	σ_E	RSD	μ_ρ	σ_ρ	RSD
0	6,37	1,07	17%	0,074	0,015	21%	2039	15,0	0,7%
15	7,71	1,42	18%	0,099	0,022	22%	2007	8,90	0,4%
30	10,05	1,31	13%	0,117	0,016	14%	2033	9,15	0,4%
60	15,52	2,29	15%	0,154	0,021	14%	2030	10,6	0,5%
90	18,93	3,92	21%	0,186	0,036	19%	1994	15,0	0,8%

The stiffness and deformation behavior in time are calculated using the compression test data. At 5% strain, the Young's modulus was calculated as a function of concrete age and equals:

$$E(t) = 0.0012 \cdot t + 0.078$$

Poisson's ratio was determined to be approximately constant in the first 90 min and was equal to 0.3 for conventional concrete. The poisons ratio of the UHPC was previously determined by several studies. The Table 4-2 presents the list of values of Poisson's ratio determined previously by some researchers. In this research, the value of 0.2 was used as the Poisson's ratio of UHPC.

Table 4-2. Values of Poisson's ratio.

Poisson's Ratio	Reference
0.2	Simon
0.16	Joh
0.21	Ahlborn
0.19	Bonneau
0.18	Graybeal
0.18	Ozyildirim

A printing speed of 1 inch/sec was defined to be constant during the process of printing. Since the printing speed is constant and the geometry of the printed structure is symmetrical on x and y axis, each layer will take the same amount of time to be printed. This time was calculated to be 75.4 seconds (1.25 minutes) per layer for the selected geometry, which means that the age of the printed layers will be increasing linearly with the average value of 1.25 minutes after each printed layer.

Figure 4-5 presents a section from the printing process. It is possible to see that after completing the printed process of the 5^{th} layer, each layer below the final layer will have different ages which will result in differences with the mechanical properties of the material such as tensile and compressive strength as well as the modulus of elasticity.

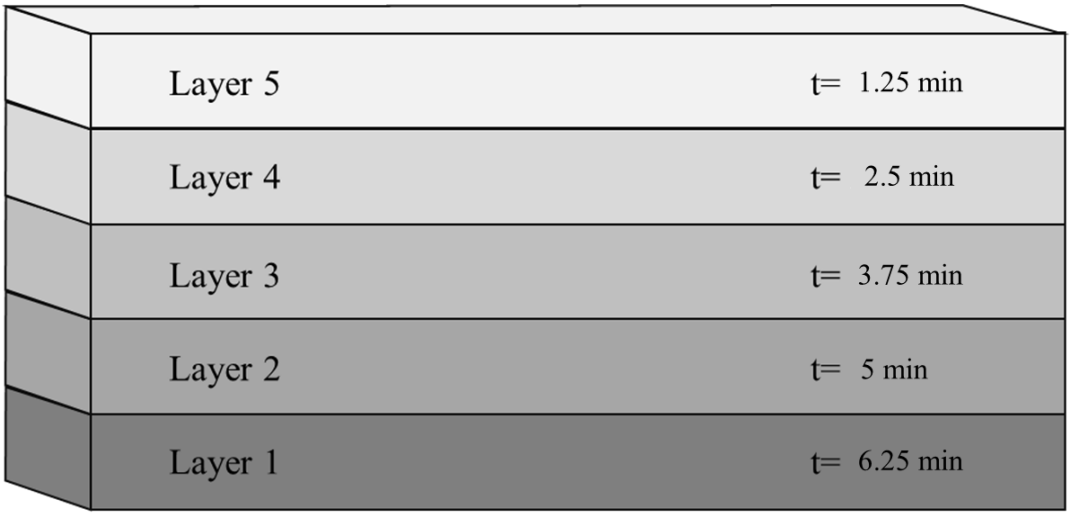

Figure 4-5. Age of the printed layers at the end of printing process of 5 layers.

Finally, using these numerical studies as well as experimental methods, a table has been created by Cervenka Consulting. Table 4-3 presents the values used by Cenvenka Consulting while developing the 3D concrete printing feature for ATENA software. This table as well as the abovementioned articles were used while calculating the input values for this research.

Table 4-3. Mechanical properties used by Cervenka Consulting while developing the 3D concrete printing feature for ATENA software. (1 kPa = 0.145 ksi)

	t=0s	t=15min	t=30min	t=60min	t=90min	t=6hour	t= ∞
E	0.074	0.099	0.117	0.154	0.186	2.3260	29900.
v	0.2						
ft	0.00280	0.00356	0.00458	0.00618	0.00803	0.02370	3.000
fc	-0.00637	-0.00709	-0.01000	-0.01550	-0.0189	-0.06120	-29.99
fc,0	-0.00425	-0.00472	-0.00669	-0.01030	-0.01260	-0.04075	-19.90
Gf	0.0293	0.03048	0.03161	0.03389	0.03615	0.06564	0.0001
εcp	1.00000	-	-	-	0.02000	-	0.0020
wd	-0.0780	-	-	-	-0.0600	-0.000532	-0.0010
γ	20						
ag	0.001						

Table 4-4. Mechanical properties used for the finite element analysis.

	t=0s	**t=15min**	**t=30min**	**t=60min**	**t=90min**	**t=6hour**	**t= ∞**
E (ksi)	0.015	0.021	0.024	0.0319	0.0386	0.48	6,200
v	0.2						
f_t *(ksi)*	0.0012	0.0015	0.00198	0.0027	0.0035	0.0102	1.3
f_c *(ksi)*	0.0037	0.0041	0.0058	0.0089	0.0109	0.0352	-17.25

5. RESULTS

Experimental test results can be categorized under 2 sections as the results related to the fresh properties of the mix and the results presenting hardened properties of the cured specimen.

5.1. Results Related to Fresh Properties

The test results related to fresh properties can be presented under four categories as extrudability test results, flowability test results, buildability test results, and the results related to open time.

5.1.1. Extrudability

Figure 4-1 shows the manually printed layers of the UHPC mix matrix and composite. Extrusion was smooth and no segregation or bleeding was observed during the test. Moreover, no deformation was observed on the printed layer during and after the extrusion, which indicates that the UHPC mix is suitable for autonomous construction purposes.

Figure 5-1. Extrudability test results of Mix Type A a) top view b) side view.

5.1.2. Workability

The spread diameters of the fresh mixes after the static flow test were very close to the bottom diameter of the brass cone (4.5 inches), which indicates that the mixes have approximately zero flow. This is desirable for 3D printing purposes since increased flow would decrease the buildability of the UHPC.

Figure 4-2 presents the flowability test procedure as well as the results. It is possible to see from the pictures that orthogonal diameters of the fresh mix are approximately 4.5 inches each, which are equal to the diameter of the brass cone used for the test. This indicates that the UHPC mix generated for 3D printing has almost no flowability in ambient conditions.

As the flow decreases, the buildability of the developed mix increases which is beneficial for the autonomous construction process. Even though low flowability is preferable for 3D printing practices, it might create extrudability and pumpability problems for the 3D printing mechanisms depending on the specific application. Therefore, the flow was gradually increased by increasing the HRWR content to reach a point where both extrudability and buildability measures were satisfied.

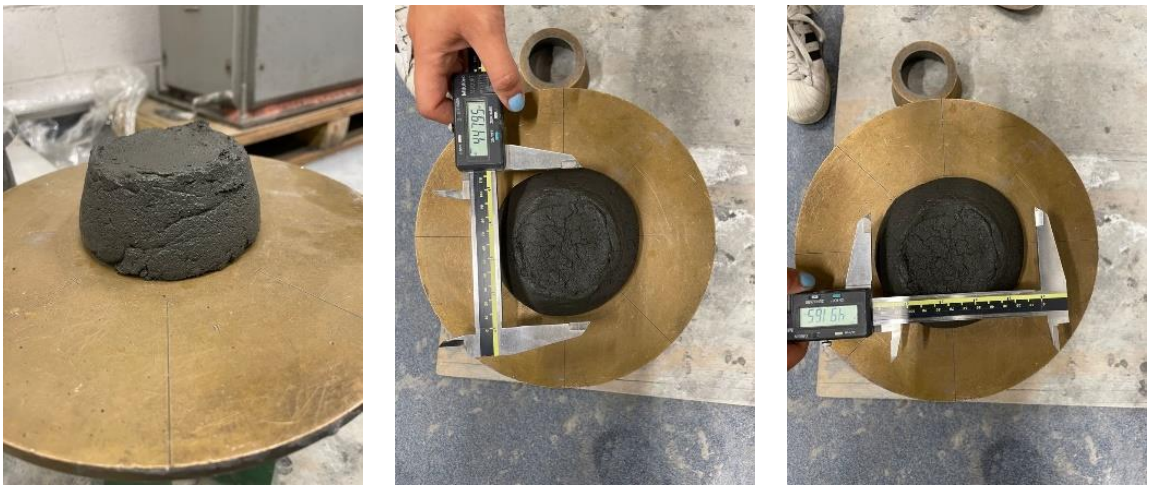

Figure 5-2. Flow test results of the 3D printable UHPC Mix Type A.

Figure 4-3 presents a comparison between the slump test results of each mix. The maximum flowability was 5.75 inches, which was achieved from the mix that has 100% extra HRWR content compared to the base design and no VMA content.

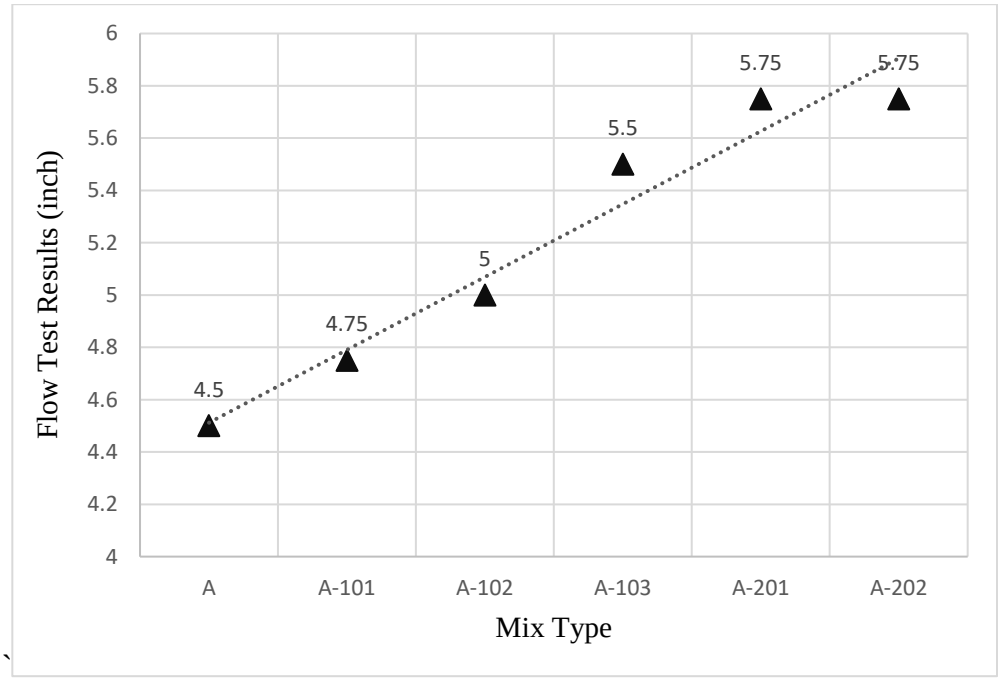

Figure 5-3. The comparison between the static slump test results.

5.1.3. Buildability

Figure 4-4 presents the photos of the sample achieved from Mix Type A under gradually increasing vertical load for testing the buildability. It can be observed that the sample was failed under the vertical load of 3.256 pounds. No visible deformation was observed until the failure of the sample.

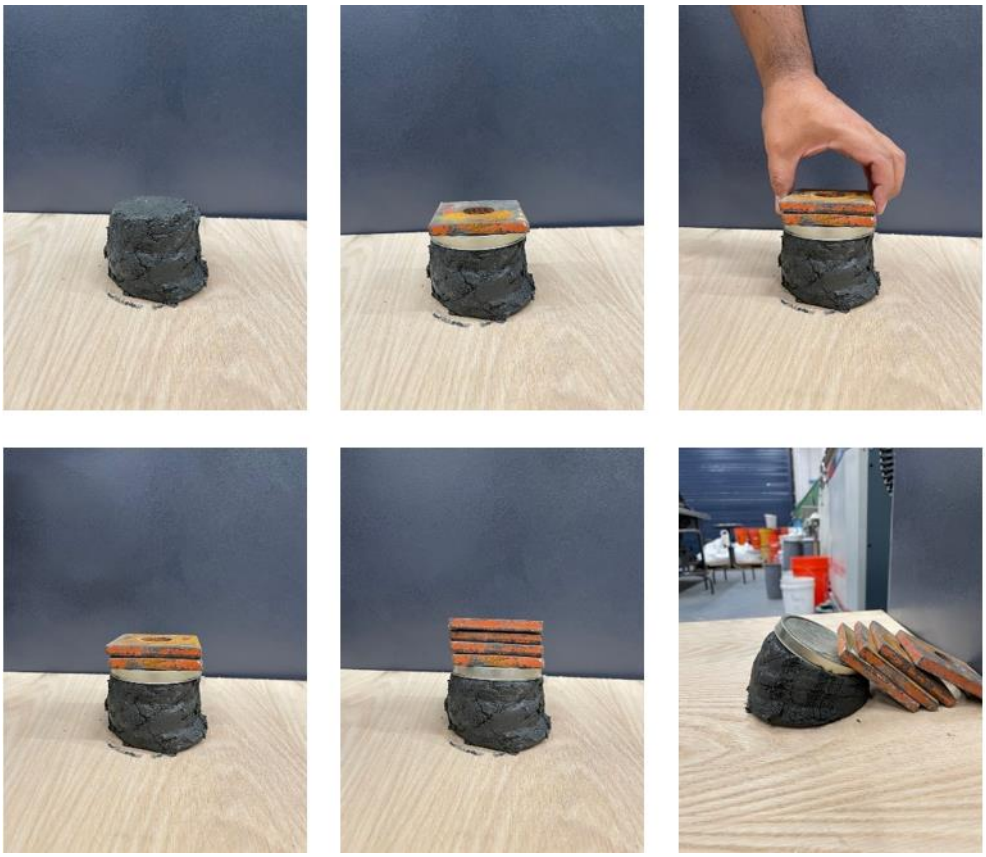

Figure 5-4: Buildability test results of the UHPC Mix Type A.

Figure 4-5 presents the buildability test results of the UHPC mixes with different amounts of HRWR. It can be seen from the results that the buildability of the mix decreases with the increased HRWR. No buildability can be measured on the mixes that have 5 inches and higher flow. Therefore, it is possible to say that, increasing the amount

of HRWR by more than 50% results in higher flowability than 5 inches and zero buildability, which makes the material unsuitable for 3D printing purposes.

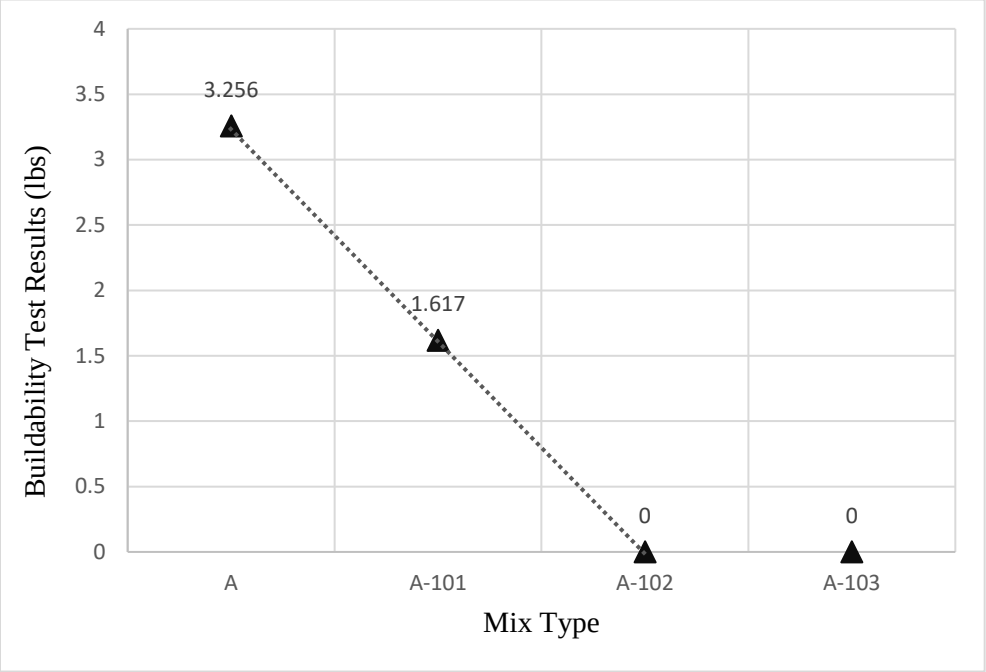

Figure 5-5. Buildability test results of the mixes with different amounts of HRWR.

In order to summarize the flowability and buildability test results and better understand the behavior of the mixes with different amounts of HRWR, two test results were combined and a suitability chart was developed. Figure 4-6 presents the suitability chart of the mixes for 3D printing purposes.

Since each 3D printing system has different challenges related to pumpability and each application has different requirements for buildability, it is not possible to come up with a single mix design that can be used for all the 3D printing applications. Instead, it is more useful to have a guideline for the mixes with different flowability and buildability

features. By using this chart, one can select the best mix that will be suitable for specific applications.

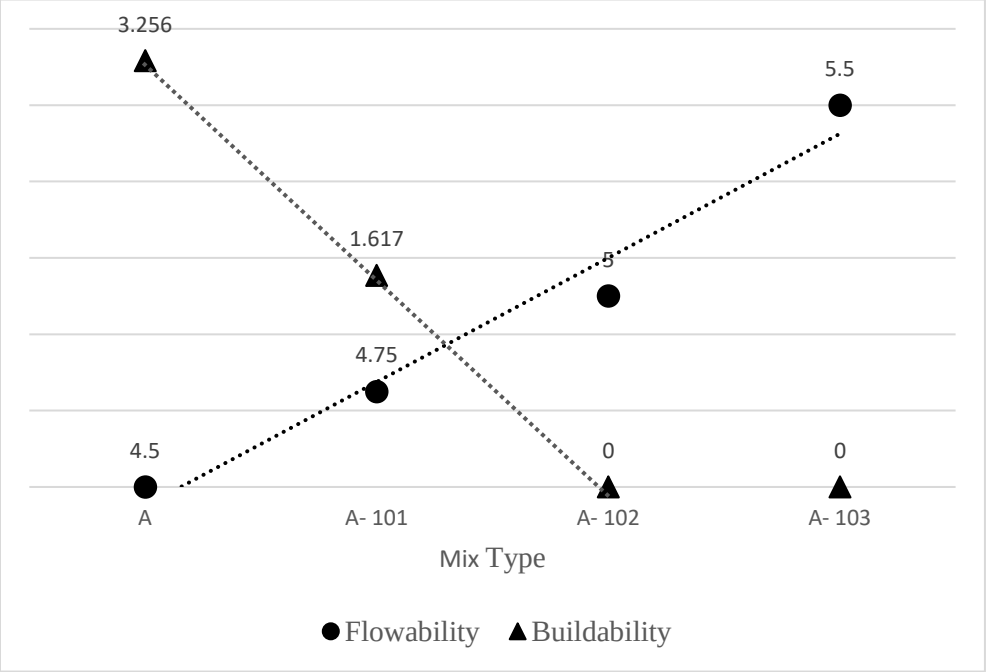

Figure 5-6. Suitability of the mixes for 3D printing.

5.1.4. Open Time

In order to measure the open time for each mix, the extrudability test was repeated every 10 minutes. All mixes were still extrudable after 20 minutes which indicates that the mixes have sufficient open time for 3D printing. Mixes with 5 inches and higher flow (Mix Type A-103, A-201, and A-202) were still extrudable after 30 minutes. However, after 25 minutes, the flowability decreased to a point that is lower than 5 inches and the mixes have started to get hardened which made them difficult to print manually. Between 25 and 40 minutes, mixes A-103, A-201 and A-202 were still extrudable but the flow

continued decreasing which made printing difficult gradually. Mixes were no longer extrudable after 40 minutes.

5.2. Results Related to Hardened Properties

Figures 5-7 through 5-9 presents the compression strength test results obtained by testing the cylindrical specimens of the mixes developed by altering the amount of HRWR. Mix A with the lowest HRWR value has the highest compressive strength value which was expected since the increased HRWR usually results in a decrease in the compressive strength of the material.

However, even though Mix A-101 has the second-lowest HRWR value, it has the lowest 28^{th}-day strength which shows that the compressive strength value is not always directly related to HRWR but also related to the entire composition of the developed material. Mix-102 has the second-highest compressive strength results with the 15.73 ksi in 28 days.

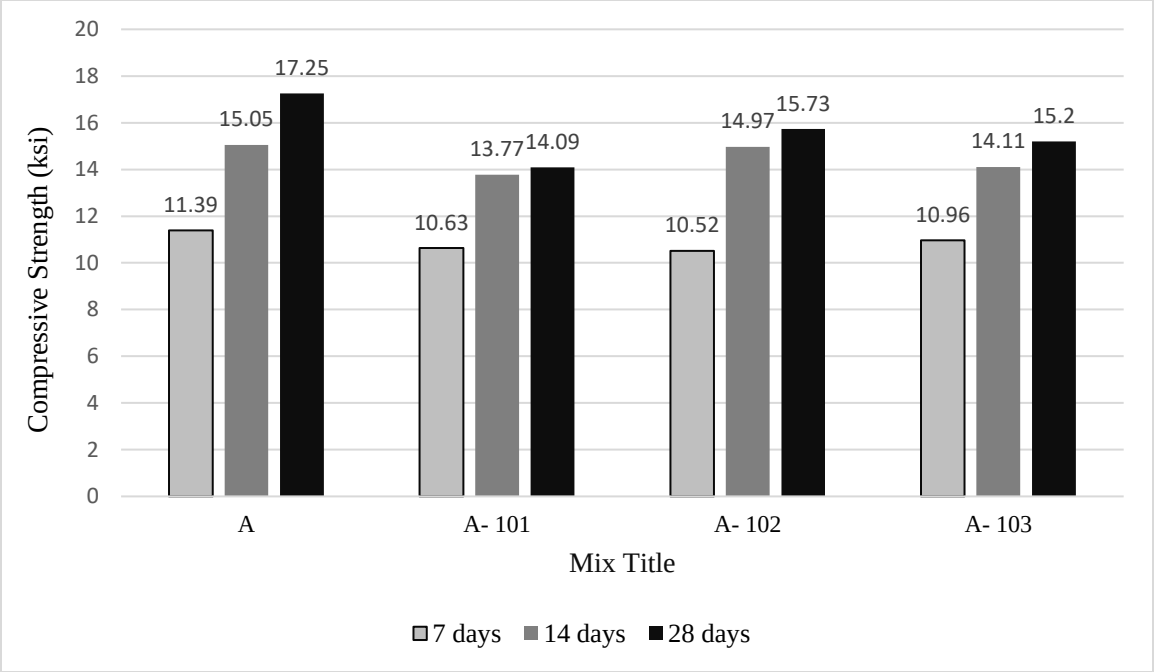

Figure 5-7. Compressive strength results of the mixes with different amounts of HRWR.

Figure 5-8 displays the compression strength test results of the mixes developed by using 0% VMA and altering the amount of HRWR. It should be noted that Mix Type A has 5% VMA content, and the information for this mix was provided for comparison purposes. It is possible to see from the figure that Mix A (the original mix with VMA) has higher compression strength results compared to Mix A-201 and Mix A-202. Mix A-201 is the mix that reached the highest compressive strength without the VMA content.

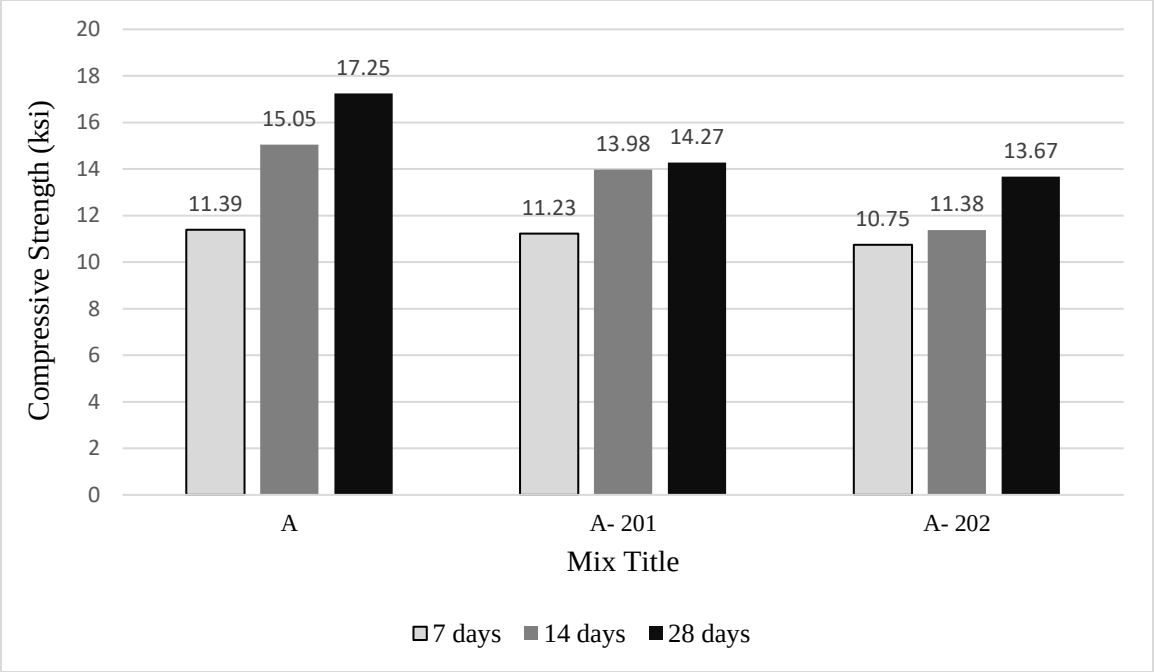

Figure 5-8. Compressive strength results of the mixes without VMA, with increasing amounts of HRWR.

Figure 5-9 presents the comparison between the compressive strength results of the same mix with and without the presence of steel fibers. For this comparison, mixes A-102 and A-S-102 were used. It is possible to see from the figure that the early strength of the mix is around 10% higher for the mix with the steel fibers. However, the compressive strength results of 14 days and 28 days are almost the same for both mixes.

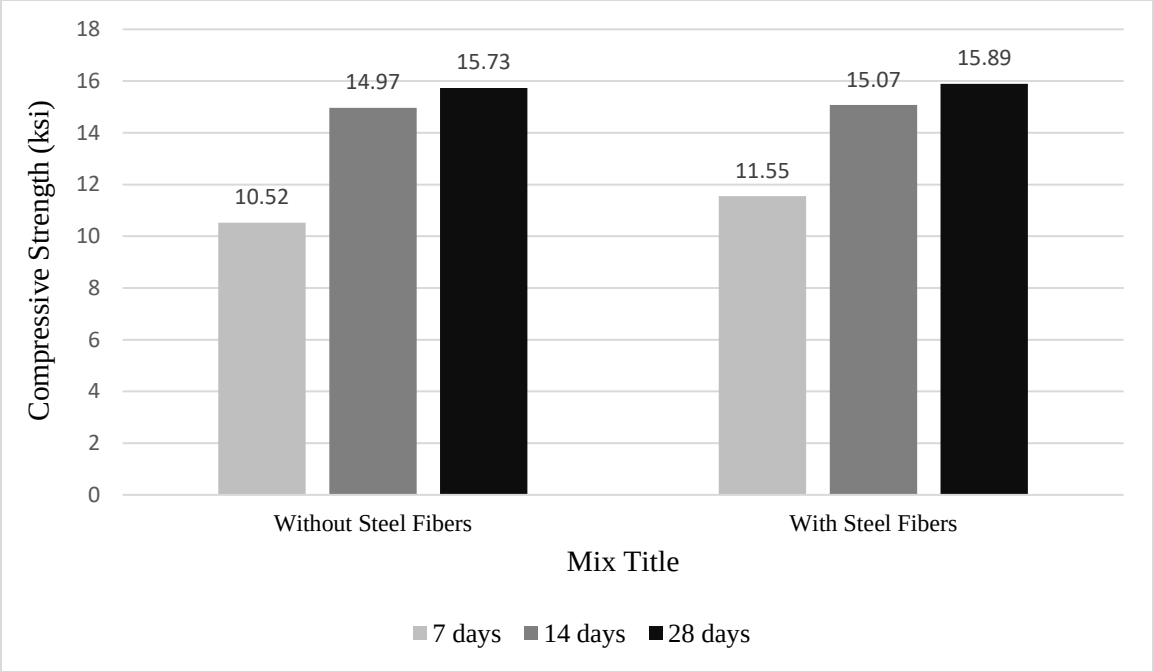

Figure 5-9. Comparison between the compression strength results of the same mix with and without steel fibers.

Even though obtaining cylindrical specimens is a simple and beneficial way to achieve compressive strength test results of the developed mixes, they cannot be used to tests for the strength of lateral directions. It is expected to see that the different directions have different strength values in 3D printing applications. Therefore, cubical specimens were used to obtain these results.

Specimens from the Mix Type A were cast in 2 stages in order to simulate the interface area between two layers. They have been tested in three orthogonal directions for 7, 14 and 28 days results. Figure 4-10 shows the testing directions in relation to the interface area between layers.

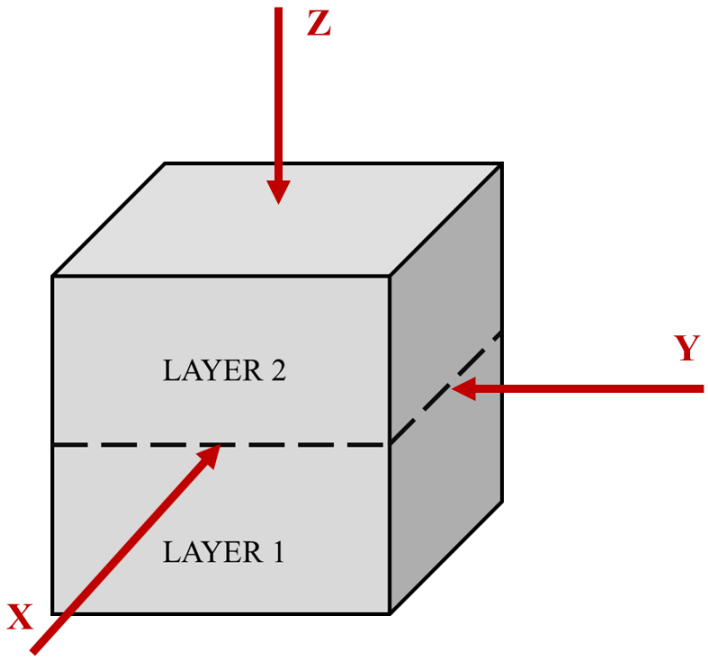

Figure 5-10. Cubical specimens were tested in three orthogonal directions.

Figure 4-11 presents the compression strength test results obtained by testing the cubical specimens. It is possible to see that direction Z, which is the orthogonal testing direction, has the highest compressive strength for 7, 14, and 28 days results due to the relationship between the testing direction and the interface area between the layers.

Layers are printed with a time delay which creates a relatively weaker area between layers. When the specimens were loaded in these two directions (X and Y directions), the interface area causes a failure sooner than the one that would achieve from the orthogonal testing direction.

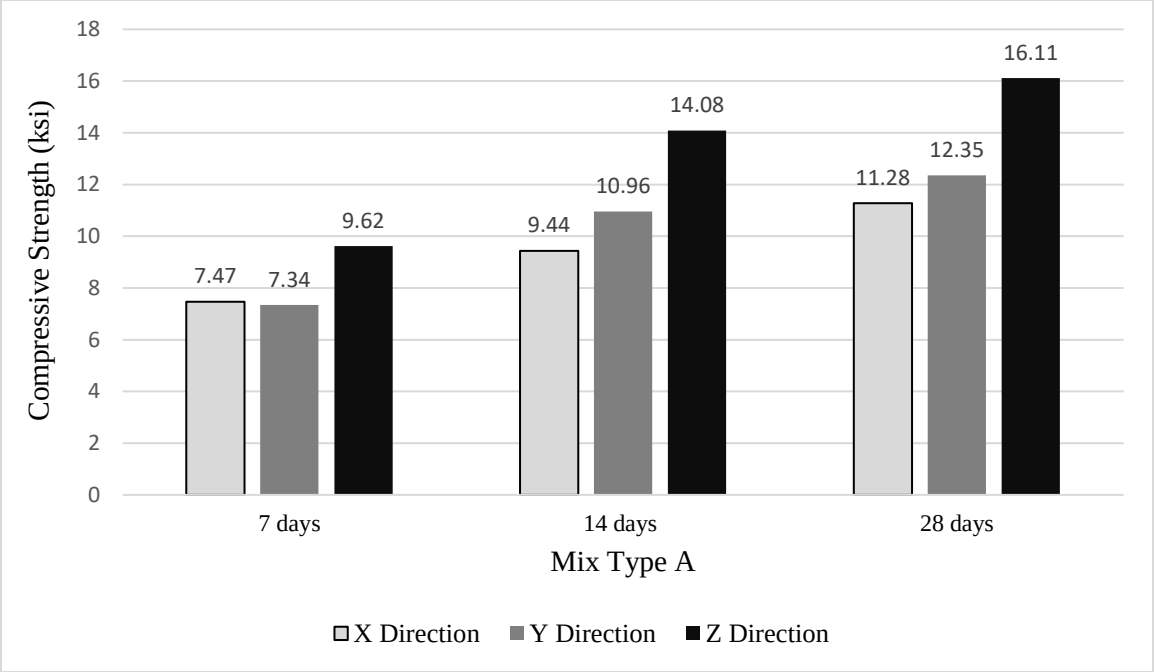

Figure 5-11. Compression strength test results obtained by testing the cubical specimens of Mix Type A.

5.3 Finite Element Analysis Results

Figure 5-12 shows the correlation between the flow value and the maximum layers to be printed without the occurrence of collapse. It is possible to see that as the flowability gets higher, the maximum number of printed layers before collapse gets lower.

This inverse relationship between the flowability of the mix and the printed layers can be explained by the instability of the printed structure. High flow and low static yield stress of the bottom layers creates stability problems which result in the demolition of the printed layers. The increase in material strength is insufficient to withstand the tension

imposed by the weight of subsequent layers. Therefore, printed structure fails due to stability related issues.

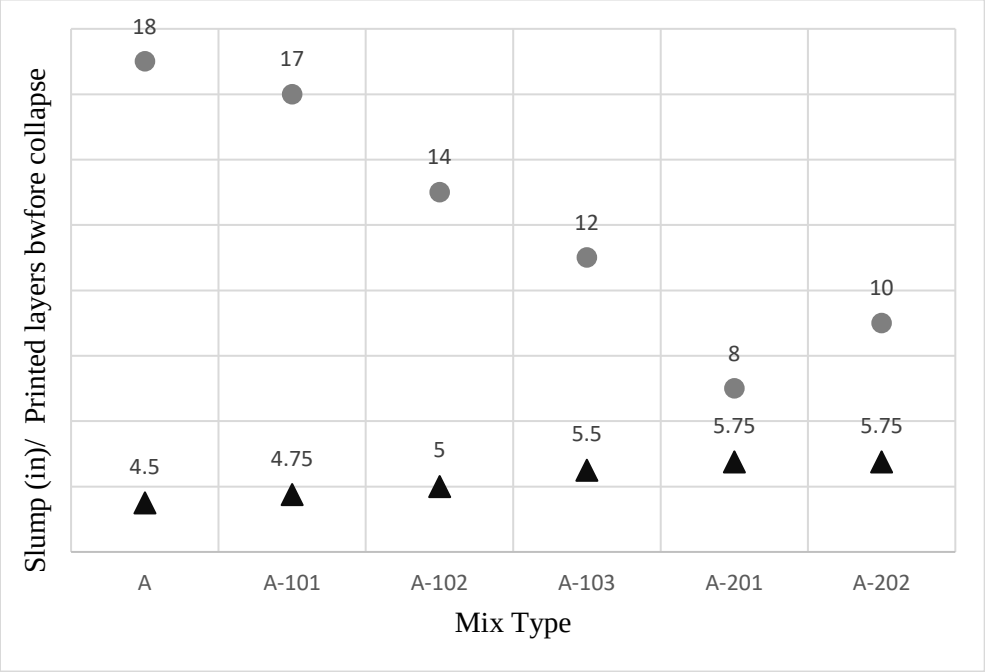

Figure 5-12. Relationship between the flowability value and maximum printed layers before collapse.

The maximum deformation was observed with the Mix Type A-201.The structure created using this mix had serious stability problems due to higher HRWR content and the lack of VMA. The optimum mix was the Mix A with the lowest flow value. It was possible to build a 18 inches tall structure using this mix without failure.

6 CONCLUSION

This study has used various measurement methods to analyze the properties of the cementitious mixes in order to develop the optimum mix design for 3D printing applications. It is found that buildability and extrudability are two crucial features for a mix to be suitable for these applications. The flowability value is a great tool for examining these measures. As the flow value increases, the maximum printed layers before collapse decreases. Therefore, the failure while printing occurs due to stability-related problems.

The Mix Type A with a flowability value of 4.5 inches and a buildability value of 3.256 lbs is the optimum matrix mix achieved in this study. This mix also reached an average 28 days compressive strength of 17.25 ksi. Moreover, this mix has passed the manual extrudability and open time tests. The Mix Type A-S-102 with the flowability value of 4.5 inches and the buildability value of 3.272 lbs was the optimum composite mix achieved.

There is no doubt that many efforts will be made in the following years and decades to produce large-scale 3-D printers and cementitious materials for these printers to be used for construction purposes. This allows concrete materials scientists to develop next-generation concrete mixes that are strong, durable, and long-lasting by including alternative binder materials and aggregates that have been enhanced through a combination of experimental research and computational modeling.

REFERENCES

[1] Occupational Safety and Health Admin. (OSHA). (2019). Commonly Used Statistics.

[2] Fadiya, O. O., Georgakis, P., & Chinyio, E. (2014). Quantitative analysis of the sources of construction waste. Journal of Construction Engineering, 2014, 9.

[3] Azizinamini, A., Rehmat, S., & Sadeghnejad, A. (2019). Enhancing resiliency and delivery of bridge elements using ultra-high performance concrete as formwork. Transportation Research Record, 2673(5), 443-453.

[4] Sadeghnejad, A., Rehmat, S., Azizinamini, A., & Caluk, N. (2019, June). Bridges ABC. In International Interactive Symposium on Ultra-High Performance Concrete (Vol. 2, No. 1). Iowa State University Digital Press.

[5] Caluk, N., Mantawy, I., & Azizinamini, A. (2019). Durable bridge columns using stay-in-place UHPC shells for accelerated bridge construction. Infrastructures, 4(2), 25.

[6] Caluk, N., Mantawy, I. M., & Azizinamini, A. (2020). Cyclic test of concrete bridge column utilizing ultra-high performance concrete shell. Transportation Research Record, 2674(2), 158-166.

[7] Li, Z., Hojati, M., Wu, Z., Piasente, J., Ashrafi, N., Duarte, J. P., ... & Radlińska, A. (2020). Fresh and hardened properties of extrusion-based 3D-printed cementitious materials: a review. Sustainability, 12(14), 5628.

[8] Standard, A. A. (2000, March). Cement and Concrete Terminology, 116R-90 (ACI 1990b). In American Concrete Institute.

[9] ASTM, C. (2020). ASTM standards. Philadelphia: American Society for Testing Materials.

[10] Buswell, R. A., De Silva, W. L., Jones, S. Z., & Dirrenberger, J. (2018). 3D printing using concrete extrusion: A roadmap for research. Cement and Concrete Research, 112, 37-49.

[11] Zhang, X., Li, M., Lim, J. H., Weng, Y., Tay, Y. W. D., Pham, H., & Pham, Q. C. (2018). Large-scale 3D printing by a team of mobile robots. Automation in Construction, 95, 98-106.

[12] Liu, Z., Li, M., Weng, Y., Wong, T. N., & Tan, M. J. (2019). Mixture Design Approach to optimize the rheological properties of the material used in 3D cementitious material printing. Construction and Building Materials, 198, 245-255.

[13] Tay, Y. W. D., Ting, G. H. A., Qian, Y., Panda, B., He, L., & Tan, M. J. (2019). Time gap effect on bond strength of 3D-printed concrete. Virtual and Physical Prototyping, 14(1), 104-113.

[14] Kazemian, A., Yuan, X., Cochran, E., & Khoshnevis, B. (2017). Cementitious materials for construction-scale 3D printing: Laboratory testing of fresh printing mixture. Construction and Building Materials, 145, 639-647.

[15] Le, T. T., Austin, S. A., Lim, S., Buswell, R. A., Gibb, A. G., & Thorpe, T. (2012). Mix design and fresh properties for high-performance printing concrete. Materials and structures, 45(8), 1221-1232.

[16] Paul, S. C., Tay, Y. W. D., Panda, B., & Tan, M. J. (2018). Fresh and hardened properties of 3D printable cementitious materials for building and construction. Archives of civil and mechanical engineering, 18(1), 311-319.

[17] Weng, Y., Li, M., Tan, M. J., & Qian, S. (2018). Design 3D printing cementitious materials via Fuller Thompson theory and Marson-Percy model. Construction and Building Materials, 163, 600-610.

[18] Arunothayan, A. R., Nematollahi, B., Ranade, R., Bong, S. H., & Sanjayan, J. (2020). Development of 3D-printable ultra-high performance fiber-reinforced concrete for digital construction. Construction and Building Materials, 257, 119546.

[19] Zhu, B., Pan, J., Nematollahi, B., Zhou, Z., Zhang, Y., & Sanjayan, J. (2019). Development of 3D printable engineered cementitious composites with ultra-high tensile ductility for digital construction. Materials & Design, 181, 108088.

[20] Javed, A., Mantawy, I. M., & Azizinamini, A. (2021). 3D-Printing of Ultra-High-Performance Concrete for Robotic Bridge Construction. Transportation Research Record, 03611981211011645.

[21] Haber, Z. B., De la Varga, I., Graybeal, B. A., Nakashoji, B., & El-Helou, R. (2018). Properties and behavior of UHPC-class materials (No. FHWA-HRT-18-036). United States. Federal Highway Administration. Office of Infrastructure Research and Development.

[22] Wolfs R.J.M. Ph.D. Thesis. Technische Universiteit; Eindhoven, The Netherlands: 2019. Experimental Characterization and Numerical Modelling of 3D Printed Concrete: Controlling Structural Behaviour in the Fresh and Hardened State.

[23] Yang, Y., Wu, C., Liu, Z., Wang, H., & Ren, Q. (2022). Mechanical anisotropy of ultra-high performance fibre-reinforced concrete for 3D printing. Cement and Concrete Composites, 125, 104310.

[24] Koh K.T., Park J.J., Ryu G.S., Kang S.T. Effect of the compressive strength of ultra-high strength steel fiber reinforced cementitious composites on curing method. J. Korean Soc. Civ. Eng. 2007;27:427–432.

[25] Vaitová, Michaela, Libor Jendele, and Jan Červenka. "3D printing of concrete structures modelled by fem." Solid State Phenomena. Vol. 309. Trans Tech Publications Ltd, 2020.

[26] Wolfs, R. J. M., F. P. Bos, and T. A. M. Salet. "Early age mechanical behaviour of 3D printed concrete: Numerical modelling and experimental testing." Cement and Concrete Research 106 (2018): 103-116.